MSNW, INC.
P.O. Box 865
San Marcos, CA 92079

STRUCTURAL INTEGRITY OF INTELLIGENT MATERIALS AND STRUCTURES

Final Technical Report

Prepared Under: Air Force Office of Scientific Research
Contract No. F49620-93-C-0052

February 1994

Prepared By: B.J. Sullivan and K.W. Buesking, MSNW, Inc.

REPORT DOCUMENTATION PAGE

Form Approved
OMB No. 0704-0188

1. AGENCY USE ONLY (Leave blank)	2. REPORT DATE	3. REPORT TYPE AND DATES COVERED
	17 Feb 94	Final Report 15Jul93-15Jan94

4. TITLE AND SUBTITLE
STRUCTURAL INTEGRITY OF INTELLIGENT MATERIALS AND STRUCTURES

5. FUNDING NUMBERS
F49620-93-C-0052

6. AUTHOR(S)
Brian J. Sullivan and Kent W. Buesking

7. PERFORMING ORGANIZATION NAME(S) AND ADDRESS(ES)
MSNW, Inc.
P.O. Box 865
San Marcos, CA 92079

8. PERFORMING ORGANIZATION REPORT NUMBER
BS-559

9. SPONSORING/MONITORING AGENCY NAME(S) AND ADDRESS(ES)
Air Force Office of Scientific Research
Bolling AFB
Washington, DC 20332-6448

10. SPONSORING/MONITORING AGENCY REPORT NUMBER
AFOSR-TR- 94 0388

11. SUPPLEMENTARY NOTES
None

12a. DISTRIBUTION/AVAILABILITY STATEMENT
Unlimited Availability
Approved for public release; distribution unlimited.

12b. DISTRIBUTION CODE

13. ABSTRACT *(Maximum 200 words)*

This report focuses on the development of micromechanical algorithms for shape memory alloy composite materials. The composite cylinders assemblage algorithm was utilized to determine the effective thermo-mechanical properties of shape memory alloy composites. The mathematical development based on this micromechanical model was coded and exercised to predict the response of shape memory alloy fiber/elastomer matrix composites to arbitrary mechanical and thermal loadings.

14. SUBJECT TERMS	15. NUMBER OF PAGES
shape memory alloys, composite materials, micromechanics	66
	16. PRICE CODE

17. SECURITY CLASSIFICATION OF REPORT	18. SECURITY CLASSIFICATION OF THIS PAGE	19. SECURITY CLASSIFICATION OF ABSTRACT	20. LIMITATION OF ABSTRACT
UNCLASSIFIED	UNCLASSIFIED	UNCLASSIFIED	UL

MSNW, INC.
P.O. Box 865
San Marcos, CA 92079

STRUCTURAL INTEGRITY OF INTELLIGENT MATERIALS AND STRUCTURES

Final Technical Report

Prepared Under: Air Force Office of Scientific Research
Contract No. F49620-93-C-0052

February 1994

Prepared By: B.J. Sullivan and K.W. Buesking, MSNW, Inc.

PREFACE

This report presents the results of an analytical modeling study performed under Air Force Office of Scientific Research Contract No. F49620-93-C-0052 during the period from July 15, 1993 to January 15, 1994. The program, entitled "Structural Integrity of Intelligent Materials and Structures," was funded as a Phase I Small Business Innovative Research contract.

The program manager and principal investigator for MSNW, Inc. was Dr. Brian J. Sullivan. Dr. Craig A. Rogers of Paradigm, Inc. served as a subcontractor to MSNW. Dr. Walter F. Jones (AFOSR/NA) served as technical monitor for this contract.

A considerable amount of assistance was provided by several individuals during the course of this research. Dr. David John Barrett of the Naval Air Warfare Center/Aircraft Division, Warminster, PA was particularly helpful in providing pertinent background material in the field of shape memory materials. Dr. Barrett was also very willing to share the results of his modeling efforts and to critique the micromechanical solutions of this work as they became available. Drs. Dimitris C. Lagoudas and James G. Boyd of Texas A&M University were also very willing to share the results of their shape memory composite micromechanical studies, including the theoretical developments and numerical solution data, even before their papers were published. The help of all of these individuals is gratefully acknowledged.

TABLE OF CONTENTS

STRUCTURAL INTEGRITY OF INTELLIGENT MATERIALS AND STRUCTURES

SUMMARY

This Phase I Small Business Innovative Research program focused on the development of micromechanical algorithms for shape memory alloy composite materials. The composite cylinders assemblage algorithm was utilized to determine the effective thermomechanical properties of shape memory alloy composites. The mathematical development based on this micromechanical model was coded and exercised to predict the response of shape memory alloy fiber/elastomer matrix composites to arbitrary mechanical and thermal loadings. Graphs illustrating the response and information acquired from the utilization of the models are contained within this report.

Equations were derived for characterizing the response of elastic fiber/shape memory alloy matrix composites, also using the composite cylinders assemblage method. This development is also presented in this final report. The success of these two different developments (i.e. shape memory alloy fiber/elastomer matrix composites and elastic fiber/shape memory alloy matrix composites) has therefore demonstrated the feasibility of utilizing the composite cylinders assemblage method to characterize the response of shape memory alloy composites.

As part of this effort, a test plan was formulated for providing data to be used in the verification of the derived mathematical models. Tests have been recommended for both monolithic shape memory alloy materials and shape memory fiber/elastomer matrix composites. The recommended tests would be used to generate sufficient data to verify both the individual constituent and unidirectional composite models for the thermomechanical response of the shape memory materials.

INTRODUCTION

In recent years, the Department of Defense and other government laboratories, and DoD prime contractors, have expended considerable resources towards the development of intelligent materials and structures. These materials and structures employing them have the ability to modify both their shape and properties in response to the thermomechanical environment. Internal and government funded research efforts at Boeing, Martin Marietta, McDonald-Douglas Aircraft, Grumman, and other companies have resulted in the development of shape memory actuators for the control of space structures, the camber control of flaps, the control of self-erectable space structures, and vibration control of jet aircraft components. Work on embedded shape memory wires by McAir, Martin Marietta, TRW, and others has been focused on the control of stress, strain, and modulus at a local level and vibration control at a macroscale level.

Shape memory alloys (SMA) have been a major element of the intelligent materials and structures research effort, and actuators for the control of structures have been designed on the basis of their unique thermomechanical behavior. Examples include robot hands and other robotic devices [1-3], radiator valves [4], helical spring actuators [5], and beam vibration control actuators [6].

In order for an alloy to exhibit the shape memory effect (SME), it must possess a crystal structure that can shift into a configuration known as martensite when it experiences certain temperatures and stresses, and then shift out of it into the austenite phase at a higher temperature. For example, if SMA wire is deformed plastically while in its low temperature martensite phase, it will regain its original configuration upon heating, through a phase transformation to the austenite crystal structure. Significant forces and displacements accompany the return to the original configuration, thereby making these materials attractive

for active control devices. Depending upon whether the SMA is in its austenite or martensite phase, it exhibits substantially different properties and has stress-strain curves of much different appearance. Figure 1 [7] shows the temperature dependent properties for the common SMA NiTi (Nitinol), while Figure 2 [8] shows the temperature dependent stress-strain curves of a typical NiTi. Figure 2 (j) through (p) also illustrates the phenomenon of pseudo- or superelasticity typical of SMAs when stressed while in their austenitic phase.

The design of SMA force and displacement actuators requires a fundamental knowledge of the behavior of these materials. There has been an extensive body of work focused on the development of constitutive models describing the thermomechanical response characteristics of SMAs. Examples include models based on the phenomenology of stress-induced martensitic phase transformation [9], SME thermodynamics and statistical physics [10], and the SME phase transformation as governed by the minimization of free energy [11].

Liang and Rogers have developed one-dimensional [12] and multidimensional [13] thermomechanical constitutive relations of SMA materials, in which an internal variable of martensitic fraction has been introduced to characterize the phase transformation of SMA. These works [12,13] have characterized the thermomechanical behavior, including phase transformations, of the SMA materials in their monolithic form, and limited quantitative and qualitative verification of their unified model has been accomplished. Other researchers have also investigated constitutive relations for monolithic SMA including Graesser and Cozzarelli [14-16], whose focus was on the description of the hysteritic phenomenon and the uses of the nickel-titanium (NiTi) SMA for energy absorbing devices. Most recently, Barrett [17] has been investigating constitutive relations of monolithic SMA

materials relative to tension-compression stress state history and the associated effects on martensite to austenite transformations.

Many applications, however, call for the embedding of SMA materials within structural components to sense and/or control the mechanical response of the structures. The interaction of the SMA materials with the surrounding materials involves complex interactions in which the temperature and phase dependence of the SMA properties will strongly affect stress and displacement boundary conditions between the embedded SMA and its host material, and the constituent residual stress states. These residual stress states, which depend on the transformation temperatures of the SMA as well as the hybrid composite processing temperature, and constituent stress states experienced during thermomechanical loading could well lead to internal damage and premature fatigue failure of the embedded SMA materials and the composite system.

There exists a small body of work which has addressed the mechanics of the interactions between the SMA elements and the host materials they are embedded within. Rogers and his co-workers [18,19] have examined at a macroscale level the behavior of composite plates with SMA reinforcements and devised a rudimentary approach [20] to predicting properties and responses of lamina and laminates employing embedded SMA actuators. More recently Boyd and Lagoudas [21] and Lagoudas, Boyd, and Bo [22] have developed micromechanical models based on the Mori-Tanaka scheme as well as finite element methods for predicting the response of unidirectional shape memory alloy fiber/elastomer matrix composites subjected to arbitrary mechanical and thermal loadings. As required by the micromechanics models, these works [21,22] have incorporated the individual constituent properties and stress states in predicting the effective response of the composite material.

OBJECTIVES

Applications exist in which composite materials employing SMA constituents are preferable to monolithic SMA materials. These are applications which involve the need for:

a) shape memory materials that transition over a narrow temperature range (e.g. approximately 1°C),

b) shape memory materials that transition at high temperatures (e.g. approximately 150°C),

c) shape memory materials with working strengths up to or exceeding approximately 690 Mpa (100 Ksi), and

d) shape memory materials with improved heat dissipation capabilities.

In order to allow designs utilizing SMA composites to be initiated, thermomechanical mathematical characterization of such materials must be developed for engineering design efforts. Accordingly, the objectives of the Phase I effort were twofold:

1) Develop rigorous micromechanical algorithms for characterizing the effective thermomechanical properties and constituent stresses and displacements of composite materials employing SMA constituents, and

2) Develop test plans for verifying the composite material models.

TECHNICAL APPROACH

This section begins with a description of the overall behavior of monolithic SMAs and the constitutive relations used to characterize these materials. Following this, the development of the micromechanical algorithm for SMA fiber/elastomer matrix unidirectional composites is presented.

Monolithic Shape Memory Alloy Materials

SMA materials exhibit the so-called "superelastic" response through a crystalline level transformation between the austenite (A) phase and the martensite (M) phase. SMA materials possess a high strain capability with the ability to remember and return to the elastic domain of the initial state (A or M) through the action of imposed stress and/or temperature. Figure 3 [23] is a schematic representation of the transformations between the parent austenite phase and the martensite phase occurring under the action of temperature changes and mechanical loads.

The martensitic fraction (ξ) is the quantity of the SMA in the martensitic phase: $\xi=0$ indicates that the material is fully austenite, while $\xi=1$ indicates that the material is fully martensite. The martensitic fraction changes as a function of temperature under stress-free conditions. This is shown schematically in Figure 4 [24], where in transitioning from austenite to martensite on cooling, the martensite phase begins to appear at the martensite start temperature M_s and the A→M transformation is complete on further cooling to the martensite finish temperature M_f. When the material is fully martensite and is heated, the austenite phase begins to appear at the austenite start temperature A_s and the M→A transformation is complete when heating is continued to the austenite finish temperature A_f.

More generally, the martensitic fraction is known to change as a function of both stress σ and temperature T. A variety of laws have been used to track the martensitic fraction $\xi(\sigma,T)$, including linear [17], exponential [21], and cosine [12]. To illustrate, for the cosine law, the martensitic fraction during M→A transformation is determined from the expression

$$\xi = \frac{1}{2}[\cos(a_A(T-A_S) + b_A\sigma) + 1] \tag{1}$$

where

$$a_A = \frac{\pi}{a_A - a_S}, \qquad b_A = -\frac{a_A}{C_A} \tag{2}$$

Similarly during A→M transformation, the martensitic fraction is computed using

$$\xi = \frac{1}{2}[\cos(a_M(T-M_f) + b_M\sigma) + 1] \tag{3}$$

where

$$a_M = \frac{\pi}{M_s - M_f}, \qquad b_M = -\frac{a_M}{C_M} \tag{4}$$

In equations (2) and (4), C_A and C_M represent material constants of the SMA material which determine the influence of stress on transition temperatures. Figure 5 [24] illustrates how transition temperatures change as a function of stress and temperature, depending on α and β. The constants C_M and C_A are related to α and β by the expressions

$$C_M = \tan\alpha, \qquad C_A = \tan\beta \tag{5}$$

Figures 6, 7 [21], and 8 show how the different transformation laws affect the shape of the monolithic SMA stress-strain curve during an isothermal tensile loading cycle which is sufficiently high to induce A→M transformation on loading, and which takes place at a

temperature which allows a portion of the SMA to return to austenite on unloading.

One-Dimensional Constitutive Modeling

The most simple form of the one-dimensional SMA constitutive equation is given by [12]

$$d\sigma = D\, d\epsilon + \Theta\, dT + \Omega\, d\xi \tag{6}$$

or

$$\sigma-\sigma_0 = D(\epsilon-\epsilon_0) + \Theta(T-T_0) + \Omega(\xi-\xi_0) \tag{7}$$

where

D = the one-dimensional Young's modulus,
Θ = the thermoelastic tensor, and
Ω = the transformation tensor.

Also the subscript 0 indicates the initial or previous values of each quantity. The transformation strain can be explained by reference to Figure 9 [12], which shows the loading portion of the stress-strain curve for a SMA material. Upon loading to the point ξ=1, the material is fully martensitic, and response continues to be elastic until plastic slip occurs within the martensitic phase. If we unload prior to plastic response, the maximum recoverable martensitic strain, or the recovery strain limit ϵ_L, can be derived from

$$\epsilon_L = -\frac{\Omega}{D} \tag{8}$$

Experimental results have shown that this recovery strain limit ϵ_L is almost a constant between M_f and A_s. This recovery strain limit is therefore considered a temperature-independent material constant and is typically specified by manufacturers of SMA materials. The

above equation thus provides an indirect approach to determine the phase transformation tensor Ω.

Equation (6) together with equations (1) and (3) determine the response of one-dimensional SMA materials such as wires. As shown in Figure 10, the Young's modulus of SMA material varies significantly. Comparison between Figure 10 and Figure 4 leads to the following relation of the martensitic fraction and the Young's modulus:

$$D = D_A + \xi (D_M - D_A) \tag{9}$$

where D_M is the Young's modulus within the martensitic phase and D_A is the modulus within the austenitic phase. A similar relationship can be written for the thermoelastic tensor Θ.

Three-Dimensional Constitutive Equations

Since the complete micromechanics of SMA composites will involve all elements of the stress and strain tensors, an extension of the one-dimensional SMA constitutive equation must be available. The works of Liang and Rogers [13], Graesser and Cozzarelli [16], and Lagoudas and his co-workers [21,22] were each examined for their possible implementation within a micromechanics algorithm. It was determined that the latter representation was most amenable to this and was therefore adapted for use in the micromechanical developments which follow. While Lagoudas employs an exponential relationship of martensitic fraction with stress and temperature, the cosine law as given by equations (1) through (4) was retained here.

In the case of a three-dimensional stress and strain state, the martensitic volume fraction dependence on stress and temperature are expressed as follows. If the M→A transformation starts from a state that has mixed austenite and martensite phases,

denoted as (ξ_M, T_M), the martensitic fraction is determined from the expression

$$\xi = \frac{\xi_M}{2}[\cos(a_A(T-A_S) + b_A\bar{\sigma}) + 1] \tag{10}$$

If the A→M transformation starts from the mixed state (ξ_A, T_A), the relevant expression is

$$\xi = \frac{1-\xi_A}{2}\cos[a_M(T-M_f) + b_M\bar{\sigma}] + \frac{1+\xi_A}{2} \tag{11}$$

In equations (10) and (11), a_A and b_A are again given by equation (2) and a_M and b_M are obtained from equation (4). Thus the three-dimensional equations for ξ were obtained from the one-dimensional forms by replacing the one-dimensional stress σ by the effective stress $\bar{\sigma}$, where $\bar{\sigma} = (\frac{3}{2}\sigma'_{ij}\sigma'_{ij})^{\frac{1}{2}}$, and the deviatoric stress σ'_{ij} is given by $\sigma'_{ij} = \sigma_{ij} - \frac{1}{3}\sigma_{kk}\delta_{ij}$.

Assuming that response will remain elastic, the three-dimensional form of the stress-strain equation may be written as

$$\sigma_{ij} = C_{ijkl}\epsilon^e_{kl} = C_{ijkl}(\epsilon_{kl} - \epsilon^t_{kl} - \alpha_{kl}\Delta T) \tag{12}$$

where ϵ^e_{ij}, ϵ_{ij}, ϵ^t_{ij}, and ΔT are the elastic strain, the total infinitesimal strain, the transformation strain, and $\Delta T = T - T_0$, where T_0 is the stress-free reference temperature. The elastic stiffness tensor C_{ijkl} and the thermoelastic expansion tensor α_{ij} are given by

$$C_{ijkl} = C^A_{ijkl} + \xi(C^M_{ijkl} - C^A_{ijkl}) \tag{13}$$

and

$$\alpha_{ij} = \alpha^{A}_{ij} + \xi(\alpha^{M}_{ij} - \alpha^{A}_{ij}) \tag{14}$$

respectively. In describing the response of SMA materials, incremental constitutive equations are used, as in (6). Taking the time derivative of (12) results in the equation

$$\dot{\sigma}_{ij} = C_{ijkl}\dot{\epsilon}^{e}_{ij} + \dot{C}_{ijkl}\epsilon^{e}_{kl} \tag{15}$$

or

$$\dot{\sigma}_{ij} = C_{ijkl}(\dot{\epsilon}_{kl} - \dot{\epsilon}^{t}_{kl} - \alpha_{kl}\dot{T} - \dot{\alpha}_{kl}\Delta T) + \dot{C}_{ijkl}\epsilon^{e}_{kl} \tag{16}$$

The three-dimensional transformation strain rate $\dot{\epsilon}^{t}_{ij}$ is obtained from

$$\dot{\epsilon}^{t}_{ij} = \Lambda_{ij}\dot{\xi} \tag{17}$$

where

$$\Lambda_{ij} = \begin{cases} -\frac{3}{2}\frac{\Omega}{D}\bar{\sigma}^{-1}\sigma'_{ij}, & \dot{\xi} > 0 \\ -\frac{\Omega}{D}\bar{\epsilon}^{t-1}\epsilon^{t}_{ij}, & \dot{\xi} < 0 \end{cases} \tag{18}$$

and where $\bar{\epsilon}^{t} = (\frac{2}{3}\epsilon^{t}_{ij}\epsilon^{t}_{ij})^{\frac{1}{2}}$ and $D = \frac{1}{2}(D^{M} + D^{A})$ is the average elastic modulus. Returning to (16), the elastic stiffness tensor C_{ijkl} and thermal expansion tensor α_{ij} are given by (13) and (14), respectively. The rates $\dot{C}_{ijkl}$ and $\dot{\alpha}_{ij}$ may be obtained from (13) and (14) using the chain rule for the time derivative of ξ, i.e.

$$\dot{\xi} = \frac{\partial \xi}{\partial T}\dot{T} + \frac{\partial \xi}{\partial \bar{\sigma}}\dot{\bar{\sigma}} \tag{19}$$

Equations (13), (14), (17), and (19) can be substituted into (16) to provide

$$\dot{\sigma}_{ij} = C_{ijkl}\dot{\epsilon}_{kl} - C_{ijkl}\alpha_{kl}\dot{T} + Q_{ij}\dot{\xi} \tag{20}$$

$$Q_{ij} = (C^{M}_{ijkl} - C^{A}_{ijkl})\epsilon^{e}_{kl} - C_{ijkl}(\alpha^{M}_{kl} - \alpha^{A}_{kl})\Delta T - C_{ijkl}\Lambda_{kl} \tag{21}$$

Collecting the terms containing $\dot{\sigma}'_{kl}$, (20) may be rewritten as

$$\dot{\sigma}_{ij} + G_{ijkl}\dot{\sigma}'_{kl} = C_{ijkl}\dot{\epsilon}_{kl} + R_{ij}\dot{T} \tag{22}$$

where

$$G_{ijkl} = -Q_{ij}\frac{\partial \xi}{\partial \bar{\sigma}}\frac{3}{2}\frac{\sigma'_{kl}}{\bar{\sigma}} \tag{23}$$

$$R_{ij} = Q_{ij}\frac{\partial \xi}{\partial T} - C_{ijkl}\alpha_{kl} \tag{24}$$

and

$$\frac{\partial \xi}{\partial \bar{\sigma}}\dot{\bar{\sigma}} = \frac{\partial \xi}{\partial \bar{\sigma}}\frac{3}{2}\frac{\sigma'_{kl}}{\bar{\sigma}}\dot{\sigma}'_{kl} \tag{25}$$

has been used. The deviatoric stress in (22) can be eliminated by using $\dot{\sigma}'_{kl} = \dot{\sigma}_{kl} - \frac{1}{3}\dot{\sigma}_{mm}\delta_{kl}$. Contracting the (ij) indices in (22) gives

$$\dot{\sigma}_{rr} = (1 - \frac{1}{3}G_{iimm})^{-1}(C_{sskl}\dot{\epsilon}_{kl} + R_{ss}\dot{T} - G_{sskl}\dot{\sigma}_{kl}) \tag{26}$$

Substituting (26) into (22) then gives the result

$$(I_{mnij} + G_{mnij})\dot{\sigma}_{ij} = C_{mnkl}\dot{\epsilon}_{kl} + R_{mn}\dot{T} \qquad (27)$$

In the results appearing later in this report, equation (27) has been used to characterize the three-dimensional stress-strain response of monolithic shape memory alloy materials. For any applied stress and temperature history, (27) is solved for the elements of the three-dimensional strain rate tensor $\dot{\epsilon}_{kl}$, which are then integrated to provide strains as a function of applied stress and temperature.

Shape Memory Alloy Composites

In addition to having access to a three-dimensional description of SMA constitutive relations, a suitable micromechanical formulation must be used to describe the mechanical and thermal response of SMA composites. The next two sections of this report contain an overview discussion of available micromechanical techniques, followed by the mathematical development of shape memory alloy composite stress-strain equations. Finally, the assumptions inherent in the shape memory alloy composite model are described at the end of this section.

Discussion of Micromechanical Methods

Thermomechanical constitutive relations of composite materials employing SMA constituents may be characterized by a number of micromechanical techniques, including the Mori-Tanaka scheme [25], as used in the works of Lagoudas and his co-workers [21,22], the composite cylinders assemblage (CCA) method [26,27], and the generalized self-consistent scheme [28,29]. Finite element analysis of repeating elements of periodic arrays, including both square and hexagonal, has also been performed to calculate effective composite properties and stress-strain relations of unidirectional composites.

The Mori-Tanaka approach is a valid micromechanical method and can be applied to the case when the reinforcement varies in shape from spheres to platelets or rods. Analysis of the results of the Mori-Tanaka approach, for the case of elastic fibers in elastic matrices, has indicated a close match with results from other micromechanical methods and with available measured data, when the volume fraction of the reinforcement phase is low, for example under 30% [30]. Beyond v_f=0.3, the Mori-Tanaka results diverge from predictions made by other schemes and with experimental data.

In the case of the CCA method [26,27], the unidirectional composite is considered as an assemblage of composite cylinders. As shown in Figure 11 [26], the composite cylinders have varying diameters but a constant d_f/d_m ratio, thus allowing the space of the composite to be completely filled in the limit as d_f/d_m becomes vanishingly small. A rigorous elasticity solution is performed for the composite or heterogeneous cylinder subjected to mechanical and thermal loadings. For these loadings, the properties of a homogeneous, transversely isotropic cylinder are sought, such that an external observer could not distinguish the response of the heterogeneous cylinder from that of the replacement homogeneous cylinder. The properties of the homogeneous, transversely isotropic cylinder are then the effective composite properties of the unidirectional composite.

The CCA approach gives closed form, exact solutions for the axially symmetric properties, including the axial or fiber direction Young's modulus E_A of the composite, the axial Poisson's ratio ν_A, the axial shear modulus G_A, the transverse bulk modulus k, and both the axial and transverse coefficients of thermal expansion (CTE) α_A and α_T. One of the drawbacks of this approach, however, is that it only bounds the transverse moduli (E_T or G_T). The generalized self-consistent scheme [28,29] provides a single closed form expression for the transverse shear modulus G_T. This

result consistently falls between the upper and lower bounds provided by the CCA method, although a rigorous proof ensuring this has not been performed.

In the generalized self-consistent scheme (GSCS), a single composite cylinder is embedded within the effective homogeneous material, as shown in Figure 12 [29]. The properties of the effective material which allow continuity of displacements and tractions across the interface between the matrix ($a \leq r \leq b$) and the effective material to be satisfied are sought.

Both the CCA and GSCS methods have been used in this work. The CCA method provides closed form exact expressions for four of the five moduli and both of the CTEs needed to fully describe a transversely isotropic material. The GSCS method has been used to provide a single closed form solution for the fifth elastic moduli. The CCA and GSCS were selected to describe the micromechanics of the SMA composites due to the relative simplicity of the physical arguments behind these methods, as well as their reliable performance at high reinforcement volume fractions.

Constitutive Equations of SMA Fiber/Elastomer Matrix Composites

Since the composite shape memory response is obtained from phase transformations occurring within the SMA fiber, the state of stress and strain in the fiber must be tracked during thermomechanical loading of the SMA composite. A convenient method for accomplishing this is to use the phase average relation [31] in rate form

$$\begin{aligned}\dot{\epsilon}^{*}_{ij} &= v_f\,\dot{\epsilon}^{f}_{ij} + v_m\,\dot{\epsilon}^{m}_{ij} \\ &= v_f(\dot{\epsilon}^{fe}_{ij} + \dot{\epsilon}^{ft}_{ij} + \alpha^{f}_{ij}\dot{T} + \dot{\alpha}^{f}_{ij}\Delta T) + v_m(\dot{\epsilon}^{me}_{ij} + \alpha^{m}_{ij}\,\dot{T})\end{aligned} \tag{28}$$

where the superscripts $*$, f, m refer to the effective composite, fiber, and matrix, respectively, and the superscripts e and t indicate elastic and transformation strain quantities, as before. The quantities v_f and v_m refer to the volume fraction of fiber and matrix, respectively, and sum to one. Using the relations

$$\dot{\epsilon}^{fe}_{ij} = S^{f}_{ijkl}\dot{\sigma}^{f}_{kl} + \dot{S}^{f}_{ijkl}\sigma^{f}_{kl} \tag{29}$$

$$\dot{\epsilon}^{me}_{ij} = S^{m}_{ijkl}\dot{\sigma}^{m}_{kl} \tag{30}$$

and also

$$\dot{\epsilon}^{ft}_{ij} = \Lambda^{f}_{ij}\dot{\xi} \tag{31}$$

equation (28) may be written as

$$\dot{\epsilon}^{*}_{ij} = v_f(S^{f}_{ijkl}\dot{\sigma}^{f}_{kl} + \dot{S}^{f}_{ijkl}\sigma^{f}_{kl} + \Lambda^{f}_{ij}\dot{\xi} + \alpha^{f}_{ij}\dot{T} + \dot{\alpha}^{f}_{ij}\Delta T) + v_m(S^{m}_{ijkl}\dot{\sigma}^{m}_{kl} + \alpha^{m}_{ij}\dot{T}) \tag{32}$$

If the phase average stress rate equation

$$\dot{\sigma}^{*}_{ij} = v_f\dot{\sigma}^{f}_{ij} + v_m\dot{\sigma}^{m}_{ij} \tag{33}$$

is used, (32) may be written in the form

$$\begin{aligned}&v_f(S^{f}_{ijkl}\dot{\sigma}^{f}_{kl} + \dot{S}^{f}_{ijkl}\sigma^{f}_{kl} + \Lambda^{f}_{ij}\dot{\xi} + \alpha^{f}_{ij}\dot{T} + \dot{\alpha}^{f}_{ij}\Delta T) \\ &+ v_m\left[S^{m}_{ijkl}\cdot\frac{1}{v_m}(\dot{\sigma}^{*}_{kl} - v_f\dot{\sigma}^{f}_{kl}) + \alpha^{m}_{ij}\dot{T}\right] = S^{*}_{ijkl}\,\dot{\sigma}^{*}_{kl} \\ &\quad + \dot{S}^{*}_{ijkl}\sigma^{*}_{kl} + \Lambda^{*}_{ij}\dot{\xi} + \alpha^{*}_{ij}\dot{T} + \dot{\alpha}^{*}_{ij}\Delta T\end{aligned} \tag{34}$$

where the total composite infinitesimal strain rate $\dot{\epsilon}^{*}_{ij}$ has been expressed in elastic, transformational, and thermal expansion strain rates. Since SMA composite transformations occur depending

upon the stress-strain history of the fiber, (34) is rearranged in terms of the unknown fiber stress rate $\dot{\sigma}^f_{ij}$ as

$$\begin{aligned} v_f (S^f_{ijkl} - S^m_{ijkl})\, \dot{\sigma}^f_{kl} &= (S^*_{ijkl} - S^m_{ijkl})\, \dot{\sigma}^*_{kl} + \dot{S}^*_{ijkl}\, \sigma^*_{kl} \\ &- v_f\, \dot{S}^f_{ijkl}\, \sigma^f_{kl} + (\alpha^*_{ij} - v_f\, \alpha^f_{ij} - v_m\, \alpha^m_{ij})\, \dot{T} \\ &+ (\dot{\alpha}^*_{ij} - v_f \dot{\alpha}^f_{ij})\, \Delta T + (\Lambda^*_{ij} - v_f\, \Lambda^f_{ij})\, \dot{\xi} \end{aligned} \tag{35}$$

where in (34) and (35),

$$\begin{aligned} S^I_{ijkl} &= (S^f_{ijkl} - S^m_{ijkl})^{-1} \\ \dot{S}^*_{ijkl} &= (S^{M*}_{ijkl} - S^{A*}_{ijkl})\, \dot{\xi} \\ \dot{S}^f_{ijkl} &= (S^{Mf}_{ijkl} - S^{Af}_{ijkl})\, \dot{\xi} \\ \dot{\alpha}^*_{ij} &= (\alpha^{M*}_{ij} - \alpha^{A*}_{ij})\, \dot{\xi} \\ \dot{\alpha}^f_{ij} &= (\alpha^{Mf}_{ij} - \alpha^{Af}_{ij})\, \dot{\xi} \end{aligned} \tag{36}$$

and

$$\dot{\xi} = \frac{\partial \xi}{\partial T}\dot{T} + \frac{\partial \xi}{\partial \bar{\sigma}^f}\dot{\bar{\sigma}}^f \tag{37}$$

and as in the previous sections on monolithic SMA, the superscripts *A* and *M* refer to the austenite and martensite response phases. Rearranging (35) and using the compliance and thermal expansion rate expressions of (36),

$$\begin{aligned} &v_f (S^f_{ijkl} - S^m_{ijkl})\, \dot{\sigma}^f_{kl} \\ &+ \left[(S^{A*}_{ijkl} - S^{M*}_{ijkl})\, \sigma^*_{kl} - v_f (S^{Af}_{ijkl} - S^{Mf}_{ijkl})\, \sigma^f_{kl} - \right. \\ &\left. (\alpha^{M*}_{ij} - \alpha^{A*}_{ij} - v_f \alpha^{Mf}_{ij} + v_f \alpha^{Af}_{ij})\, \Delta T - (\Lambda^*_{ij} - v_f \Lambda^f_{ij}) \right] \dot{\xi} \\ &= (S^*_{ijkl} - S^m_{ijkl})\, \dot{\sigma}^*_{kl} + (\alpha^*_{ij} - v_f \alpha^f_{ij} - v_m \alpha^m_{ij})\, \dot{T} \end{aligned} \tag{38}$$

Then substituting (37) into (38) and rearranging further,

$$
\begin{aligned}
&v_f(S^f_{ijkl}-S^m_{ijkl})\,\dot{\sigma}^f_{kl}+\left[(S^{A*}_{ijkl}-S^{M*}_{ijkl})\,\sigma^*_{kl}-v_f(S^{Af}_{ijkl}-S^{Mf}_{ijkl})\,\sigma^f_{kl}\right.\\
&\left.-(\alpha^{M*}_{ij}-\alpha^{A*}_{ij}-v_f\alpha^{Mf}_{ij}+v_f\alpha^{Af}_{ij})\,\Delta T-(\Lambda^*_{ij}-v_f\,\Lambda^f_{ij})\right]\frac{\partial\xi}{\partial\bar{\sigma}^f}\dot{\bar{\sigma}}^f\\
&=(S^*_{ijkl}-S^m_{ijkl})\,\dot{\sigma}^*_{kl}+\left\{(\alpha^*_{ij}-v_f\alpha^f_{ij}-v_m\alpha^m_{ij})-\left[(S^{A*}_{ijkl}-S^{M*}_{ijkl})\,\sigma^*_{kl}\right.\right.\\
&\left.\left.-v_f(S^{Af}_{ijkl}-S^{Mf}_{ijkl})\,\sigma^f_{kl}-(\alpha^{M*}_{ij}-\alpha^{A*}_{ij}-v_f\alpha^{Mf}_{ij}+v_f\alpha^{Af}_{ij})\,\Delta T-(\Lambda^*_{ij}-v_f\,\Lambda^f_{ij})\right]\frac{\partial\xi}{\partial T}\right\}\dot{T}
\end{aligned}
\tag{39}
$$

where

$$
\begin{aligned}
\dot{\bar{\sigma}}^f=\;&\dot{\sigma}^f_{11}\cdot\frac{2\sigma'^f_{11}-\sigma'^f_{22}-\sigma'^f_{33}}{2\bar{\sigma}^f}+\dot{\sigma}^f_{22}\cdot\frac{-\sigma'^f_{11}+2\sigma'^f_{22}-\sigma'^f_{33}}{2\bar{\sigma}^f}\\
&+\dot{\sigma}^f_{33}\cdot\frac{-\sigma'^f_{11}-\sigma'^f_{22}+2\sigma'^f_{33}}{2\bar{\sigma}^f}+\dot{\sigma}^f_{12}\cdot\frac{3\sigma^f_{12}}{\bar{\sigma}^f}\\
&+\dot{\sigma}^f_{23}\cdot\frac{3\sigma^f_{23}}{\bar{\sigma}^f}+\dot{\sigma}^f_{31}\cdot\frac{3\sigma^f_{31}}{\bar{\sigma}^f}
\end{aligned}
\tag{40}
$$

At this point $\dot{\bar{\sigma}}^f$ from (40) is substituted into (39), and the resulting simultaneous equations are solved for the elements of the stress rate tensor $\dot{\sigma}^f_{kl}$. The fiber stress rate tensor $\dot{\sigma}^f_{kl}$ is then used in (40) to compute the fiber effective stress rate $\dot{\bar{\sigma}}^f$, after which the martensitic fraction rate is determined from (37). Finally, the composite strain rate tensor $\dot{\epsilon}^*_{ij}$ is obtained from the sum of the composite elastic, thermal, and transformation strain rates as

$$
\dot{\epsilon}^*_{ij}=S^*_{ijkl}\dot{\sigma}^*_{kl}+\dot{S}^*_{ijkl}\sigma^*_{kl}+\alpha^*_{ij}\dot{T}+\dot{\alpha}_{ij}\Delta T+\Lambda^*_{ij}\dot{\xi}
\tag{41}
$$

or, using (36)

$$\dot{\epsilon}^*_{ij} = S^*_{ijkl}\dot{\sigma}^*_{kl} + (S^{M^*}_{ijkl} - S^{A^*}_{ijkl})\dot{\xi}\sigma^*_{kl} + \alpha^*_{kl}\dot{T} + (\alpha^{M^*}_{ij} - \alpha^{A^*}_{ij})\dot{\xi}\Delta T + \Lambda^*_{ij}\dot{\xi} \tag{42}$$

The procedure outlined above enables all elements of the composite strain rate tensor $\dot{\epsilon}^*_{ij}$ to be determined for an arbitrary three-dimensional composite stress rate $\dot{\sigma}^*_{kl}$ and an applied temperature and temperature rate history. Strains as a function of time, and therefore stress and temperature, are determined by integrating (42).

Assumptions of Shape Memory Alloy Composite Model

Prior to the completion of the SMA composite model, several assumptions must be made to complete the development. First, it is assumed that the stress-free phase transition temperatures (M_f, M_s, A_s, and A_f) are unchanged from those of the monolithic SMA material. Note that the composite stress-free temperature is theoretically at or in the vicinity of the temperature at which the SMA composite is cured. When cooled from this process temperature, the composite is in a state of residual stress which, in and of itself, induces changes in the phase transition temperatures due to the dependence of these temperatures on stress (see Figure 5).

Secondly, it is assumed that composite phase transformation occurs when the SMA fiber changes phase. Since the composite can effectively transition only when its SMA constituents undergo a phase transition, this is a very reasonable assumption. In order to implement this, the fiber stress state must be computed from the applied composite stresses using the phase average stress model. This requirement was implemented in the development of the preceding section.

Lastly, the standard CCA model assumption that the fiber axial strain is equal to the composite axial strain must be utilized. This leads to the determination of the composite thermoelastic tensor since the fiber recovery strain limit ϵ_L^f must equal the composite recovery strain limit ϵ_L^*, thereby providing the equation

$$-\frac{\Omega^f}{D^f} = \epsilon_L^f = \epsilon_L^* = -\frac{\Omega^*}{D^*} \tag{43}$$

where D^f is the average fiber Young's modulus and D^* is the average composite axial Young's modulus. Thus the quantity $-\frac{\Omega^*}{D^*}$ required for the computation of Λ_{ij}^* is available from (43).

RESULTS OF MATHEMATICAL MODELS

Results for both the monolithic and composite shape memory alloy materials have been obtained using the models detailed above. Note that all remaining results in this report have been generated using the cosine transformation rules of equations (10) and (11). Results are shown first for the monolithic SMA materials. These solutions have been obtained by integrating (27) using the fourth-order Runge-Kutta method of numerical integration, with Gil's technique applied to minimize round-off errors [32].

Results for Monolithic Shape Memory Materials

The axial stress-strain response of monolithic Nitinol (NiTi) shape memory alloy under isothermal loading conditions is shown in Figure 13. The material properties used to represent NiTi are shown on this figure and in Table 1. Curves showing the response obtained at three separate temperatures (28°C, 35°C, and 51°C) are indicated on this graph. The different temperatures affect the austenite elastic limit on initial loading, with isothermal loading at the highest temperature (51°C) requiring the most stress prior to initiating A→M transition. Isothermal loading at 51°C also results in the highest stress for the A→M transition to be completed. Upon unloading at 51°C, M→A transition begins at approximately 100 Mpa, and the M→A transition begins to occur at about 30 Mpa for unloading at 35°C. Complete unloading in the case of 28°C does not result in any M→A phase transition.

The $\Delta L/L$ versus temperature response of monolithic NiTi SMA under stress-free conditions is shown in Figure 14. The temperature history used to obtain the response was T=29→0→55→29°C. The shape of this thermal strain curve is easily understood when the phase transition temperatures are considered. Upon cooling from 29°C, the $\Delta L/L$ curve is initially linear until the temperature reaches 23°C, the martensite start temperature. Further cooling

induces continued A→M transformation which is finally complete by 5°C. At this temperature the curve resumes a linear form with a smaller slope than the initial (29°C→23°C) cooling portion, since α^M is considerably smaller than α^A (6.6 versus 11 ppm/°C). On heating from 0°C, the thermal strain is linear with temperature at a rate of 6.6 ppm/°C until the temperature reaches 29°C, the austenite start temperature. The curve is nonlinear from 29°C to 51°C when it returns to a linear form, since the austenite finish temperature has been reached and the material is now fully austenite. For the rest of the temperature history (51→55→29°C), the thermal strain versus temperature curve is linear with a slope of 11 ppm/°C, the CTE of the austenite phase.

Figure 15 illustrates the effect of isothermally loading a monolithic NiTi SMA beyond the elastic stress limit to a value of 110 MPa, at which point the material has experienced a small percentage of A→M phase transformation. The material is then unloaded elastically. Upon reloading, additional A→M phase transition will not occur until the stress exceeds 110 MPa. This indicates that the stress required to induce further transformation has "hardened." Additional unload/reload cycles are also shown on this plot for higher values of martensitic fraction, with a final unload cycle at ξ=1. Note that the slope of the unload/reload curves becomes increasingly smaller, reflecting the decrease in elastic modulus as the material becomes increasingly more martensitic.

The shape memory effect for the monolithic NiTi SMA is illustrated in Figures 16 and 17. Figure 16 shows the first step of the process, which is an isothermal stress cycle of sufficient intensity to induce complete (ξ=1) phase transformation. Note that, as in Figure 13, no M→A phase transformation occurs on unloading for $T=T_o$=28°C. Figure 17 shows that as the temperature is increased from 28°C, the material returns to the austenite phase

by the time the temperature reaches 51°C. The phase transition is accompanied by a full strain recovery.

Results for SMA Fiber/Elastomer Matrix Composites

The procedure outlined in the section on constitutive equations of SMA fiber/elastomer matrix composites has been used to obtain the results which follow. As in the case of the monolithic SMA, the fourth-order Runge-Kutta method with Gil's modification has been performed to integrate (42), thus providing the composite strain history as a function of applied stress and temperature.

Figures 18 and 19 show the results of the CCA method of this report for the case of an isothermal tensile stress applied in the fiber direction at 35°C. Figure 18 shows the axial stress versus axial strain, while Figure 19 shows the axial stress versus transverse strain. In these two figures the CCA method results are compared to both the Mori-Tanaka (M-T) solution and finite element results obtained from the analysis of a square periodic array [22]. The M-T and finite element results have incorporated the exponential phase transition rule, while the CCA results shown here have utilized the cosine transformation rule. Principal differences in the results of the three methods include the stress and strain at which the composite fully transitions to martensite and the stress and strain at which M→A transitioning begins upon unloading. On loading, the elastic stress limit appears identical for the CCA and M-T solutions and the response immediately after this point differs in the same fashion in which exponential and cosine transformation rule results differ for monolithic SMAs. On continued loading, the M-T solution appears to reach full martensite much earlier than either the finite element or CCA results, which have the same stress at full transition, although their composite strains at full martensite are different. The CCA results indicate greater compliance than the finite element results, but some of this may be due to the use of a square

periodic array as opposed to a hexagonal repeating element model. On complete unloading, all three methods give approximately the same axial and transverse composite strains. Generally speaking, the differences between all three curves are due to variations in the manner in which fiber and matrix stress states are computed, which is different for each micromechanical technique. The overall character of the three curves is, however, very similar.

Figure 20 shows the composite level stress-free thermal response curve for the NiTi fiber/elastomer matrix, with 29°C considered to be the stress-free temperature of the unidirectional constituents. This means that at any temperature other than the initial 29°C state, the composite constituents will experience stresses due to their thermal expansion mismatch. On cooling, the composite begins to transition to martensite at a temperature slightly above 23°C, and the transformation appears complete by 15°C. This is as opposed to the NiTi fiber stress-free transition temperatures of M_s=23°C and M_f=5°C, and the differences are entirely due to the thermally induced stresses in the NiTi fiber due to the CTE mismatch between the fiber and the matrix. Since the composite has not experienced any M→A transformation on heating from 0°C, the thermal strain is linear with temperature and will be slightly smaller when it returns to 29°C.

The unidirectional composite shape memory effect (SME) for a 0.2 fiber volume fraction composite is illustrated in Figures 21 and 22. As in the monolithic material, the first step of the SME is an isothermal stress cycle that induces phase transformation which is not recovered on unloading. Figure 22 shows the second step of the process, which is the complete recovery of the transformation strain on heating. The small strain remaining is a thermal expansion strain. There are two important aspects to the SME results, both of which appear in Figure 22. First, the composite M→A transition temperatures are considerably higher than

the NiTi stress-free A_s and A_f temperatures. This is entirely due to the stress in the fiber induced from thermal mismatch. Secondly, unlike the thermal recovery in the case of the monolithic material shown in Figure 17, the composite recovery occurs almost instantaneously once the M→A phase transformation begins. This was first observed by Boyd and Lagoudas [21], who noted that once transformation is initiated, a self-perpetuating cycle of fiber effective stress decreases leading to ξ decreases occurred. As the reductions in fiber effective stresses took place, the effective composite A_f temperature dropped to the point where full M→A transformation occurred at essentially A_s.

The situation changes, however, as the fiber volume fraction increases. Results for the composite SME for a 0.6 fiber volume fraction SMA composite are shown in Figures 23 and 24. As shown in Figure 24, the transformation is not instantaneous for the higher fiber volume fraction composite. This is due to the fact that as the fiber volume fraction increases, the fiber effective stress on complete unloading of the composite is considerably reduced from its value in the low fiber volume fraction composites, as shown in Figure 25. The lower fiber effective stress allows a more gradual transition and a recovery which resembles that of the monolithic material. Effective unidirectional NiTi fiber/elastomer matrix composite austenitic phase temperatures as a function of the NiTi fiber volume fraction, obtained from simulating the composite shape memory effect, are shown in Figure 26.

TEST PLANS FOR MODEL VERIFICATION

In order to verify the mathematical models, testing must be performed on both monolithic SMA materials and composites made using SMA constituents. There is a need for multi-dimensional constitutive relation development which differentiates between tensile and compressive normal stresses, since there is some concern [17,21] that the sign of the fiber axial stress may affect the manner in which phase transformations occur. For example, results such as those shown in Figure 26, which depend entirely on the fiber effective stress with no regard to whether the fiber is in tension or compression, may not be valid. Considerable confidence exists for SMA constitutive laws in which the SMA material is in a state of tension. The same level of confidence does not exist for SMA materials either entirely in compression or experiencing tensile-compressive stress cycling. Since the SMA fiber will be in residual compression on cooling from composite fabrication for the high CTE elastomer matrix materials, more information about monolithic SMA material response for non-tensile load states must be available, even before the composite SMA material model can be verified.

Once monolithic SMA material testing has been concluded, composite tests can be conducted, the most important of which will focus on fiber dominated responses. Mechanical loading in the fiber direction, composite stress-free fiber direction strain versus temperature, and shape memory effect tests should all be conducted.

It should also be noted that the SMA fiber composition should be well characterized with respect to the Ni and Ti percentages in the Nitinol alloy. Obviously, the exact same composition Nitinol must be present in the NiTi fibers as was used to characterize the monolithic material response. In addition, the response of the elastomer matrix used in the composite fabrication and testing

should be completely measured at all anticipated strain levels expected in the composite testing.

Table 2 contains the recommended test matrix for verification of monolithic and composite shape memory material models.

CONCLUSIONS AND RECOMMENDATIONS

All technical objectives stated as goals at the initiation of the Phase I program were met during performance of the program. The analytical developments required to complete this effort resulted in significant new information which adds to the state-of-the-art of the relatively new field of micromechanical modeling of SMA composites. The following paragraphs summarize the primary conclusions of the Phase I program.

The feasibility of using the composite cylinders assemblage (CCA) micromechanical method to characterize the response of shape memory alloy (SMA) composites was demonstrated in the Phase I effort. Equations were derived for characterizing the response of unidirectional SMA fiber/elastic matrix composites utilizing the CCA method. Analytical results using the CCA approach compared favorably to results for identical problems obtained by Mori-Tanaka and finite element analyses. The model was also exercised to predict stress-free composite SMA thermal strain versus temperature response, and simulations of the shape memory effect (SME) were conducted for several different fiber volume fraction composites. These numerical solutions pointed out that stress-free SME thermal recovery occurs isothermally at low fiber volume fractions. This result can be explained in the context of the mathematical phase transition laws; however it may not be physically realistic.

Additional equations were derived for characterizing the response of elastic fiber/shape memory alloy matrix composites, also using the CCA method. This development is contained in the report appendix.

The mathematical modeling performed here indicates the promise of shape memory composites in meeting needs identified by ARPA [33,34] in the area of shape memory actuators, including SMA materials with a narrow transition range, SMA materials that

transition at high temperatures, and SMA materials with improved heat dissipation capabilities. As shown in Figure 26, the narrow transition range materials may be achievable with SMA composites if the transformation law dependence on the SMA constituent effective stress is correct. SMA materials that transition at high temperatures are also possible using SMA composites, due to the high residual stresses from processing. The transition temperatures indicated in Figure 26 were derived using a composite stress-free temperature of only 25°C. A more realistic stress-free temperature defined by processing conditions will result in even higher transition temperatures. Lastly, SMA materials with improved heat dissipation capabilities may be possible using SMA composites through the placement of high conductivity particles or whiskers, such as graphite. Discontinuous forms of high conductivity graphite are necessary, as opposed to graphite fibers, due to the high strain capability of the SMA and the low strain-to-failure properties of graphite fibers.

A test plan was formulated to provide data for verification of both the monolithic material models and the composite SMA models. As noted above, some concern exists regarding the validity of the current constitutive modeling of SMA materials, particularly when compressive stress states exist. Since composite materials employing SMA constituents will experience residual compressive stresses, further work must be performed to validate or correct existing monolithic SMA constitutive models. After this has been accomplished, any required changes to the SMA composite micromechanics can be performed, at which point the SMA composite test data can be used to validate the micromechanical models.

REFERENCES

1. Nakano, Y., "Hitachi's Robot Hand," Robotics Age, Vol. 6, pp. 18-20, 1984.

2. Schetky, L., "Shape Memory Effect Alloys for Robotic Devices," Robotics Age, Vol. 6, pp. 13-17, 1984.

3. Honma, D., Miwa, Y. and Iguchi, N., "Application of Shape Memory Effect to Digital Control S Actuator," Bulletin of JSME, Vol. 27, pp. 1737-1742, 1984.

4. Schetky, L., "Shape Memory Alloys," Scientific American, Vol. 241, pp. 74-82, 1979.

5. Baz, A., Iman, K. and McCoy, J., "The Dynamics of Helical Shape Memory Actuators," J. Intell. Mater. Syst. and Struct., Vol. 1, pp. 105-133, 1990.

6. Baz, A., Iman, K. and McCoy, J., "Active Vibration Control of Flexible Beams Using Shape Memory Actuators," J. Sound and Vibr., Vol. 140, pp. 437-456, 1990.

7. Jackson, C.M. et al., "55-Nitinol - The Alloy with a Memory: Its Physical Metallurgy, Properties and Applications," NASA-SP-5110, p. 91, 1972.

8. Funakubo, H., "Shape Memory Alloys," Gordon and Breach Science Publishers, 1987.

9. Warlimont, H. et al., "Review: Thermoelasticity, Pseudo-elasticity and the Memory Effects Associated with Martensitic Transformations; Part 3: Thermodynamics of Kinetics," J. Mater. Sci., Vol. 9, pp. 1545-1555, 1974.

10. Achenbach, M., Atanackovic, T. and Muller, I., "A Model for Memory Alloys in Plane Strain," Int. J. Solids Struct., Vol. 22, pp. 171-193, 1986.

11. Tanaka, K. and Nagaki, S., "A Thermomechanical Description of Materials with Internal Variables in the Process of Phase Transformation," Ingenieur-Archiv, Vol. 51, pp. 287-299, 1982.

12. Liang, C. and Rogers, C.A., "One-Dimensional Thermomechanical Constitutive Relations for Shape Memory Materials," J. Intell. Mater. Syst. and Struct., Vol. 1, pp. 207-234, 1990.

13. Liang, C. and Rogers, C.A., "The Multi-Dimensional Constitutive Relations of Shape Memory Alloys," Proc. AIAA 32nd Structures, Structural Dynamics and Materials Conf., April 1991.

14. Graesser, E.J. and Cozzarelli, F.A., "Shape Memory Alloys as New Materials for Aseismic Isolation," J. of Engrn. Mech., ASCE, Vol. 117, No. 11, pp. 2590-2608, November 1991.

15. Graesser, E.J. and Cozzarelli, F.A., "Fully Cyclic Hysteresis of a Ni-Ti Shape Memory Alloy," Proceedings of Damping '93, WL-TR-93-3104, pp. ECB-1 to ECB-28, June 1993.

16. Graesser, E.J. and Cozzarelli, F.A., "A Proposed Three-Dimensional Model for Shape Memory Alloys," submitted to the Journal of Intelligent Material Systems and Structures, 1993.

17. Barrett, J.D., " A One-Dimensional Constitutive Model for Shape Memory Alloys," to be presented at the 1994 International Conference on Intelligent Materials, Williamsburg, VA, June 5-8, 1994; also submitted to the Journal of Intelligent Material Systems and Structures, 1994.

18. Rogers, C.A., Liang, C. and Barker, D., "Dynamic Control Concepts Using Shape Memory Alloy Reinforced Plates," Proc. U.S. ARO Workshop on Smart Materials, Structures and Mathematical Issues, Blacksburg, VA, 1988.

19. Rogers, C.A., Liang, C. and Jia, J., "Behavior of Shape Memory Alloy Reinforced Plates," Proc. AIAA 30th Structures, Structural Dynamics and Materials Conf., 1989.

20. Jia, J. and Rogers, C.A., "Formulation of a Mechanical Model for Composites with Embedded SMA Actuators," J. Mech. Design, 1989.

21. Boyd, J.G. and Lagoudas, D.C., "Thermomechanical Response of Shape Memory Composites," submitted to the Journal of Intelligent Materials and Structures, 1993.

22. Lagoudas, D.C., Boyd, J.G. and Bo, Z., "Micromechanics of Active Mechanics," presented at the 1993 ASME Winter Annual Meeting, New Orleans, LA, December 1993.

23. Uchino, K., "Shape Memory Effect Associated With the Forced Phase Transition in Antiferrolectrics," Proceedings of MRS International Meeting on Advanced Materials, Vol. 9, Shape Memory Materials, pp. 489-503, May 31-June 3, 1988.

24. Rogers, C.A., "A Review of Shape Memory Alloys and Their Composites," Paradigm, Inc. report to MSNW, Inc., January 12, 1994.

25. Mori, T. and Tanaka, K., "Average Stress in Matrix and Average Elastic Energy of Materials with Misfitting Inclusions," Acta Metallurgica, Vol. 21, pp. 571-574, 1973.

26. Hashin, Z., "Theory of Fiber Reinforced Materials," NASA CR-1974, March 1972.

27. Hashin, Z., "Analysis of Properties of Fiber Composites with Anisotropic Constituents," J. Appl. Mech., Vol. 46, No. 3, pp. 543-550, September 1979.

28. Christensen, R.M. and Lo, K.H., "Solutions for Effective Shear Properties of Three-Phase Sphere and Cylinder," J. Mech. Phys. Solids, Vol. 37, pp. 315-330, 1979.

29. Christensen, R.M., Mechanics of Composite Materials, Chapter 2, John Wiley & Sons, New York, NY, 1979.

30. Christensen, R.M., "A Critical Evaluation for a Class of Micromechanics Models," J. Mech. Phys. Solids, Vol. 38, No. 3, pp. 379-404, 1990.

31. Barrett, D.J. and Buesking, K.W., "Temperature Dependent Nonlinear Metal Matrix Laminate Behavior," NASA CR-4016, September 1986.

32. James, M.L., Smith, G.M. and Wolford, J.C., Applied Numerical Methods for Digital Computation, Chapter 6, Fourth Edition, Harper Collins College Publishers, New York, NY, 1993.

33. DARPA Small Business Innovative Research Solicitation, Topic No. 91-056: Shape Memory Development for Actuators.

34. Jones, G. (ARPA), Personal communication with D.J. Barrett (NAWC/AD), February 1992.

Table 1. SMA fiber and elastomer matrix properties

NiTi Material Properties

$D^A = 30.0 \times 10^3\ MPa$

$D^M = 13.0 \times 10^3\ MPa$

$\nu = 0.33$

$\alpha^A = 11.0 \times 10^{-6}/°C$

$\alpha^M = 6.6 \times 10^{-6}/°C$

$M_s = 23°C$

$M_f = 5°C$

$A_s = 20°C$

$A_f = 51°C$

$C^M = 11.3\ MPa/°C$

$C^A = 4.5\ MPa/°C$

$\Omega = -0.91 \times 10^3\ MPa$

Polymer Material Properties

$D = 2.0 \times 10^3\ MPa$

$\nu = 0.45$

$\alpha = 75 \times 10^{-6}/°C$

Table 2. Test Matrix for Verification of Monolithic and Composite Models

MATERIAL	LOADING TYPE / REPLICATIONS [+]				
	Tension	Tension - Compression Cycle	Compression Cycle	Compression - Tension Cycle	Temper-ature Cycle
Monolithic SMA	2-3	2-3	2-3[•]	2-3	2-3
Elastomeric Matrix	2-3	-	2-3	-	2-3
SMA/Elastomer Composite					
$v_f = 0.2$	2-3	2-3	2-3	2-3	2-3
$v_f = 0.35$	2-3	2-3	2-3	2-3	2-3
$v_f = 0.5$	2-3	2-3	2-3	2-3	2-3

[+] Third Replication of Test Used If Needed For Tie Breaker
[•] These Tests To Be Performed With And Without Lateral Constraint

Tests To Demonstrate Shape Memory Effect (Isothermal Loading, Thermal Recovery) To Be Performed On Monolithic And Composite SMA Materials

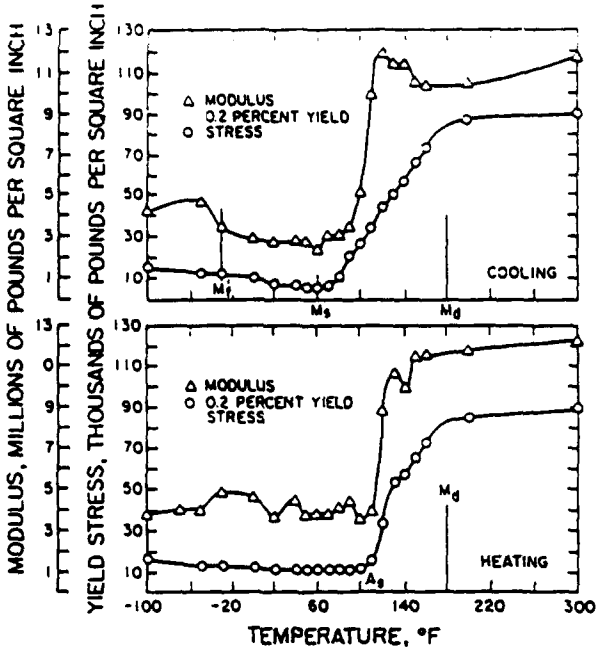

Figure 1. The Effect of Temperature on the Yield Stress and Elastic Modulus of Shape Memory Alloys [7].

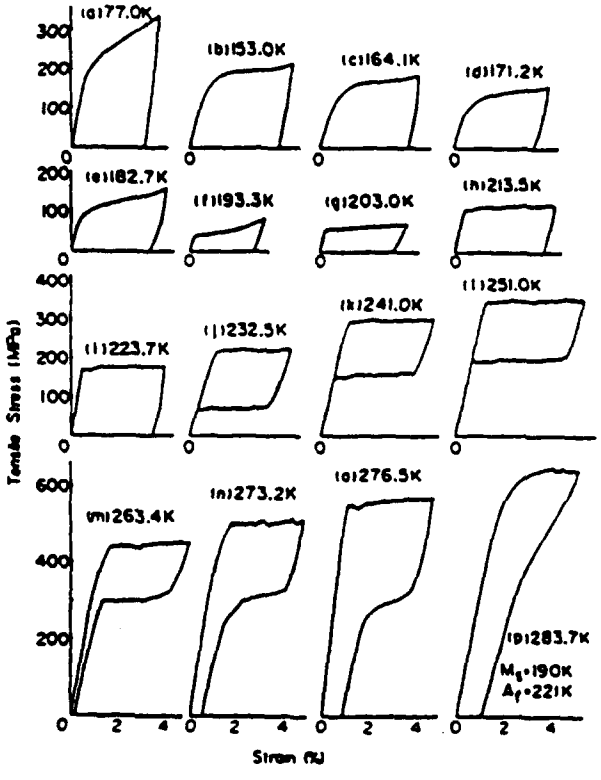

Figure 2. Stress-Strain Behavior with Unload Illustrating Elastic, Plastic and Superelastic Responses [8].

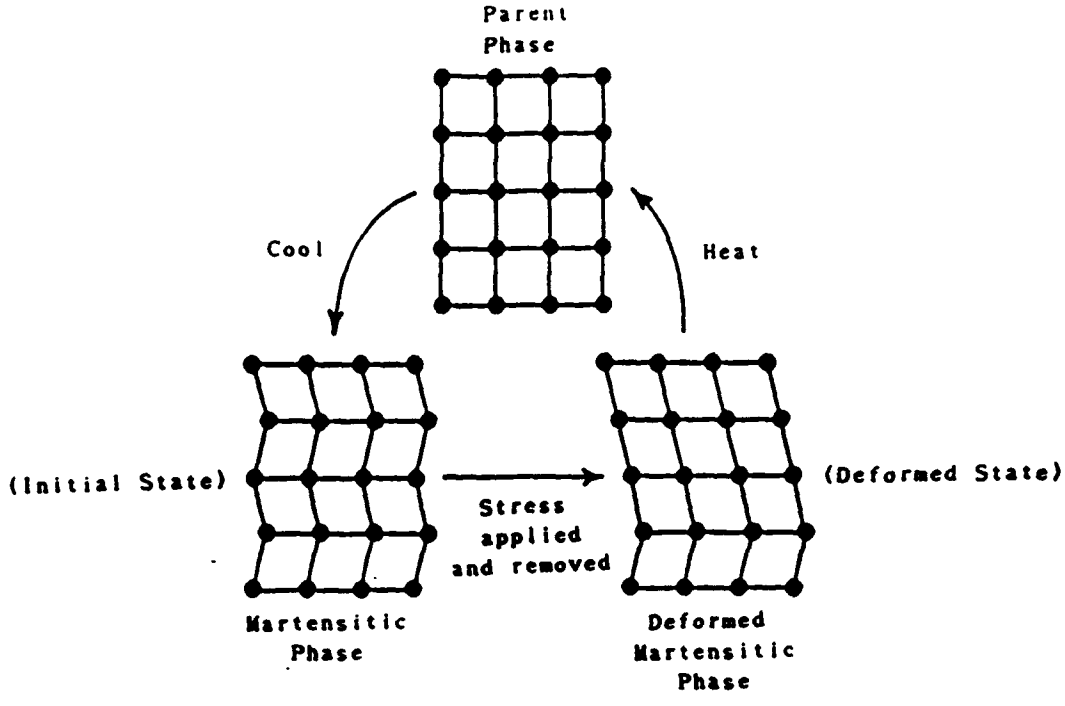

Figure 3. Mechanisms For Shape Memory Effect in Shape Memory Alloys [23].

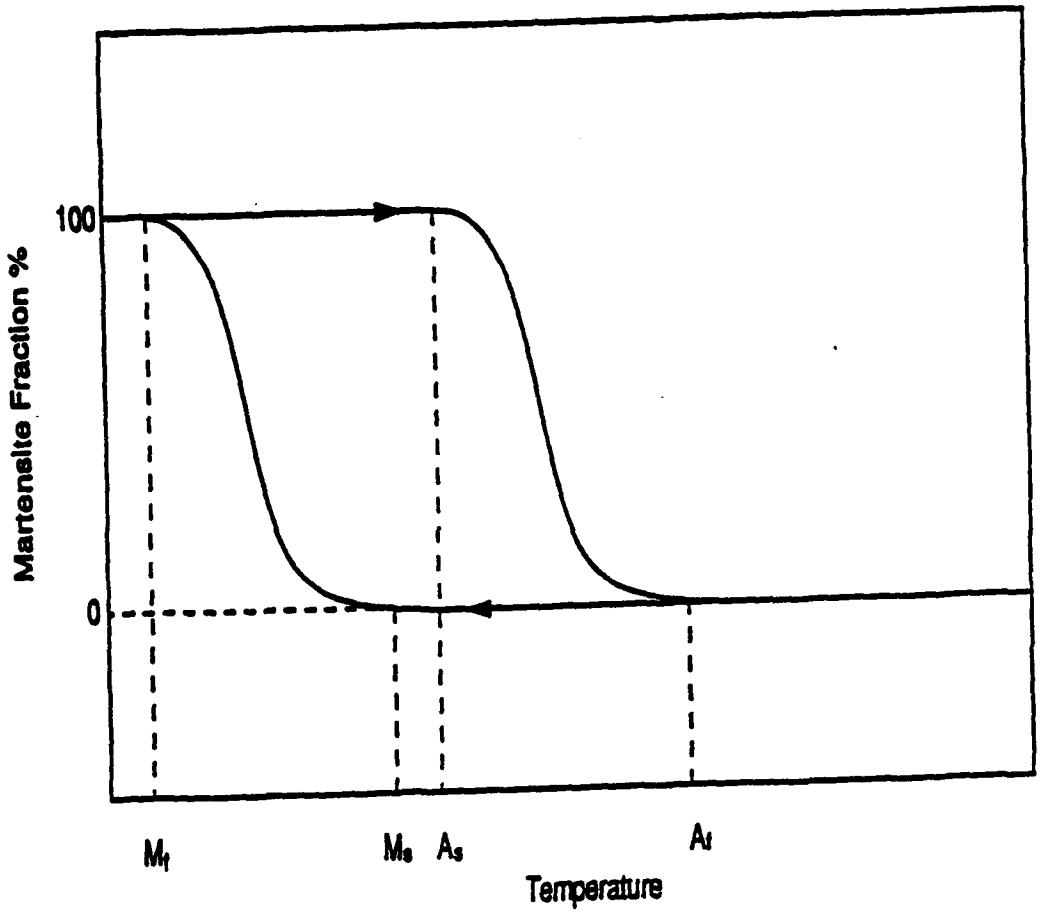

Figure 4. A Schematic Diagram of the Martensite Fraction Vs. Temperature [24].

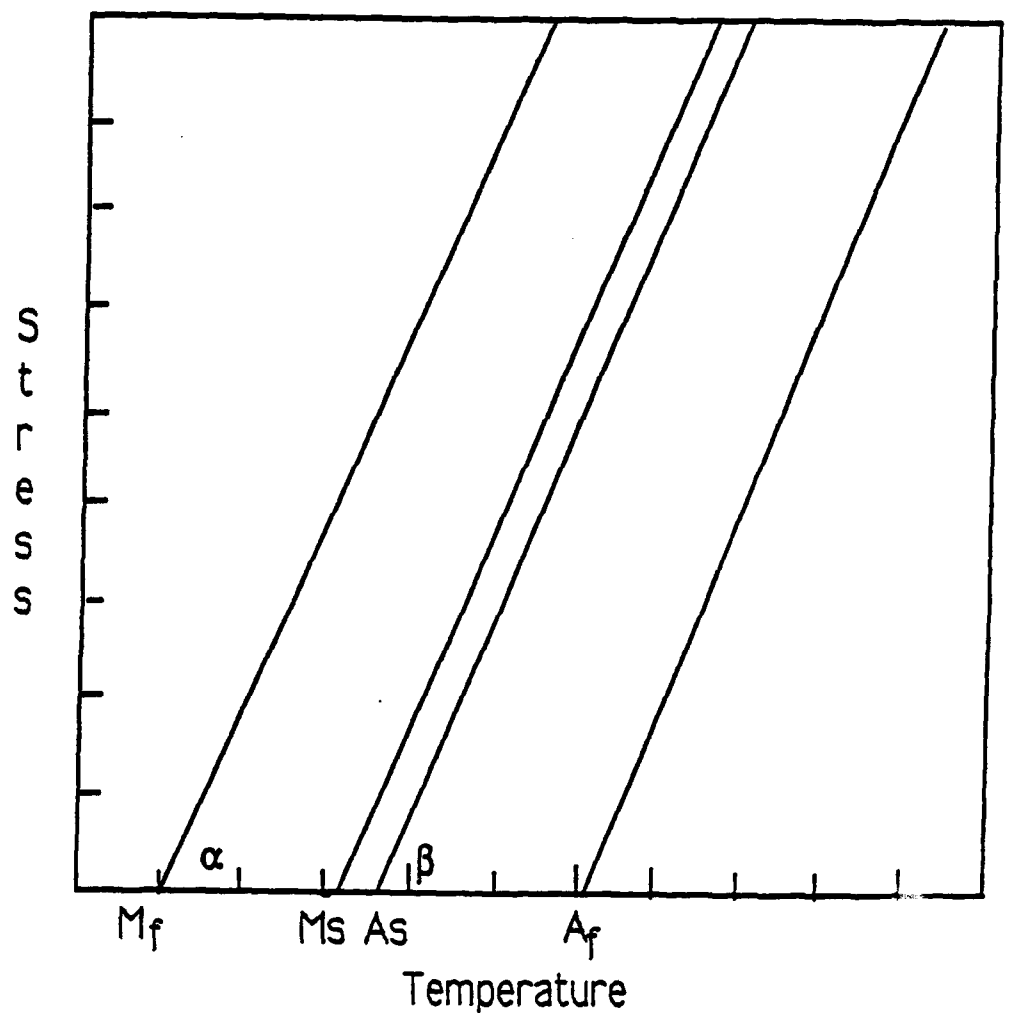

Figure 5. A Schematic Diagram of Transition Temperatures Vs. Applied Stress [24].

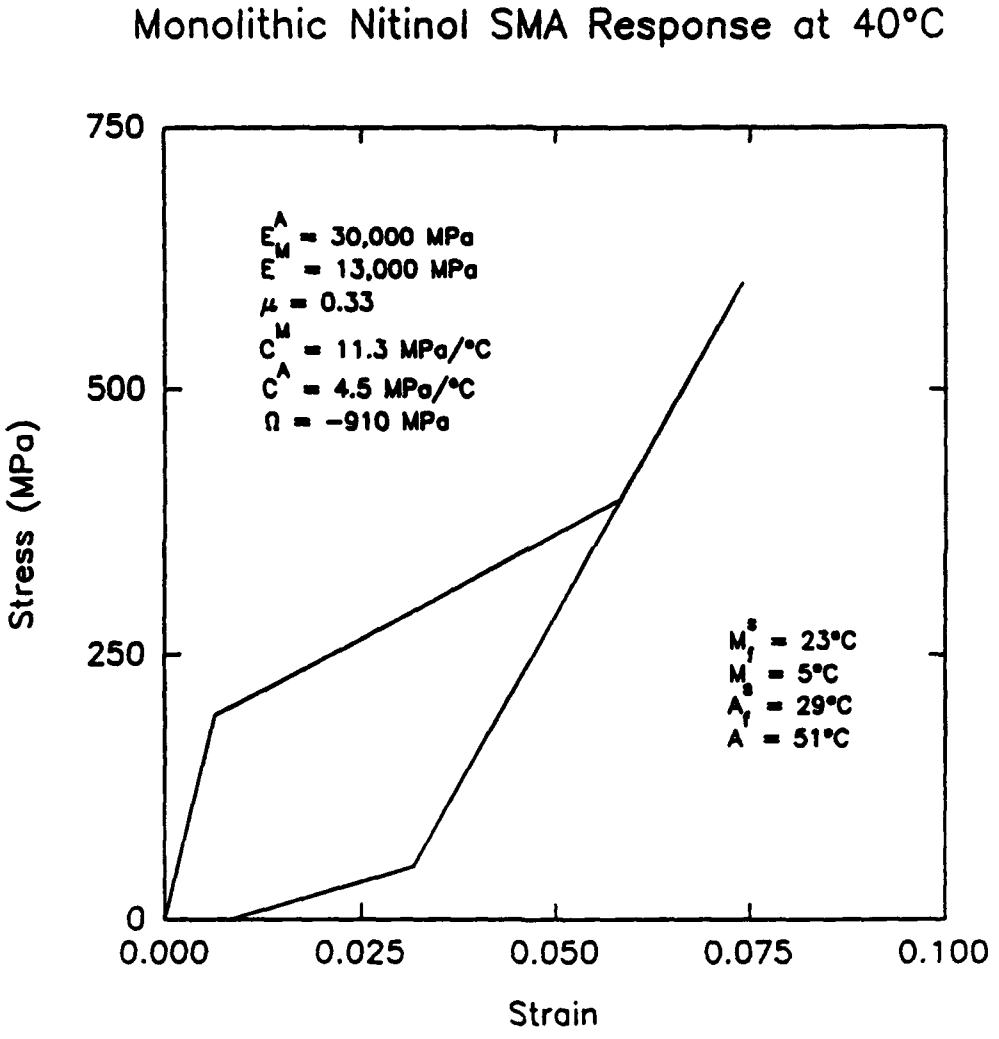

Figure 6. Monolithic Nitinol SMA Isothermal Stress-Strain Response Using Linear Phase Transformation Rule.

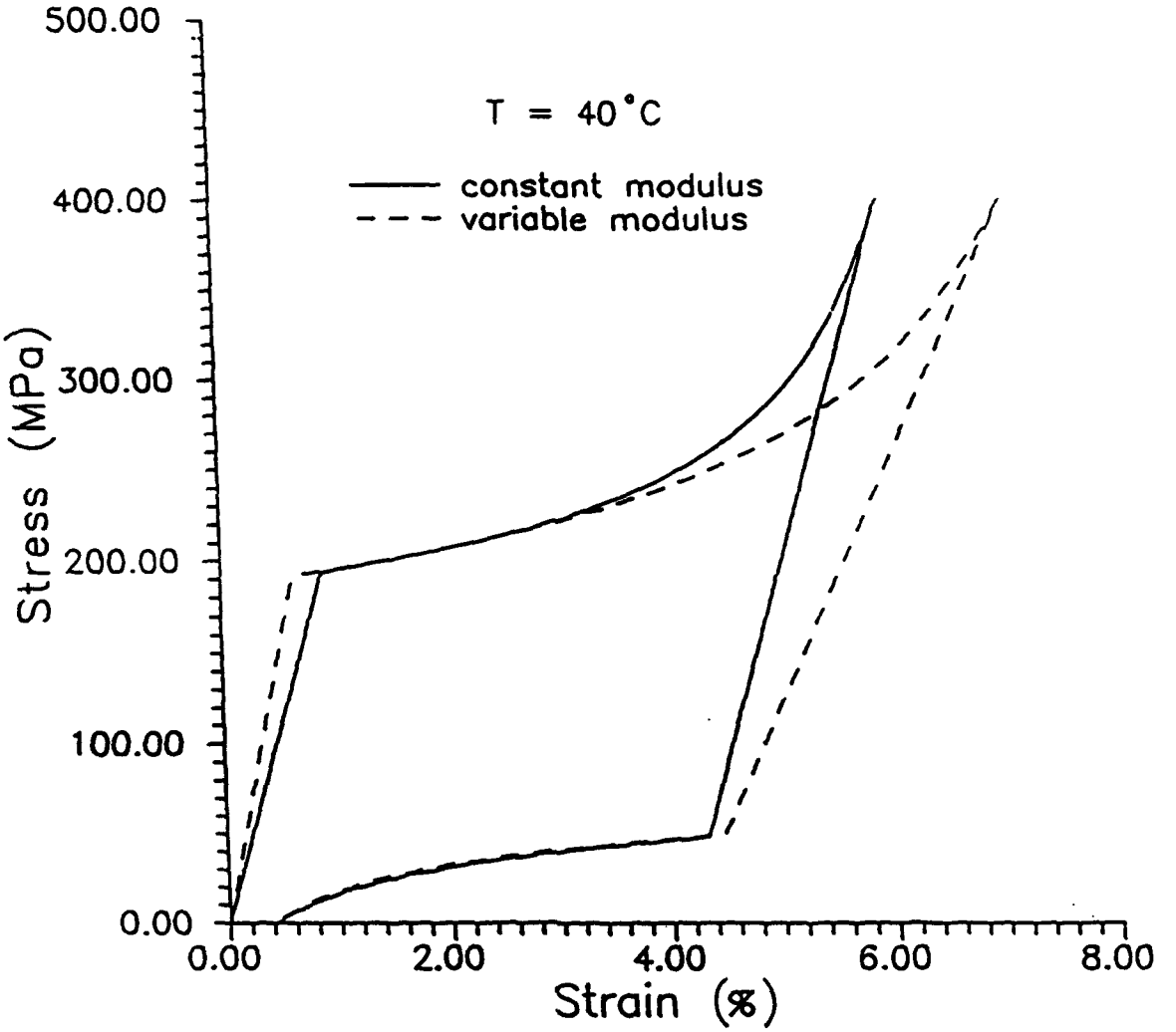

Figure 7. Monolithic Nitinol SMA Isothermal Stress-Strain Response Using Exponential Phase Transformation Rule [21].

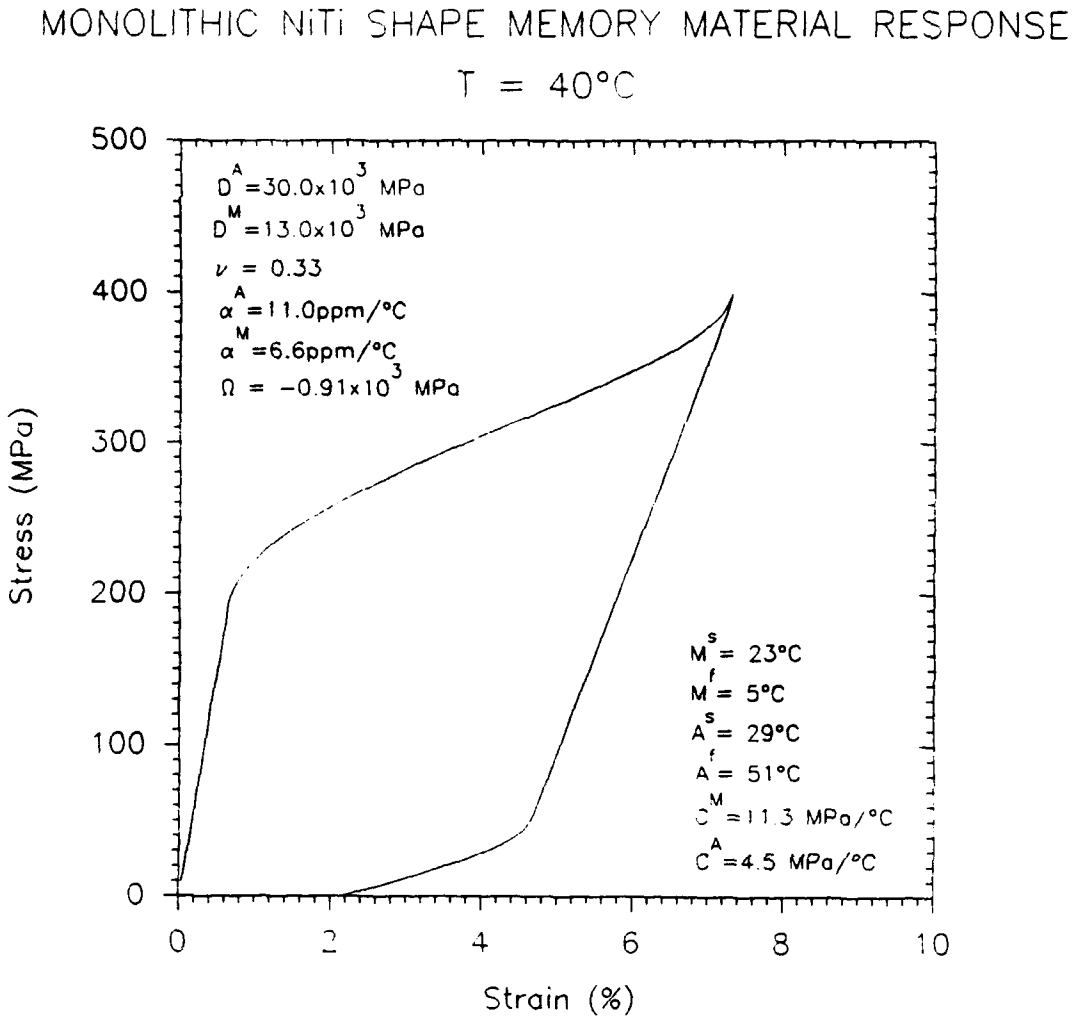

Figure 8. Monolithic Nitinol SMA Isothermal Stress-Strain Response Using Cosine Phase Transformation Rule.

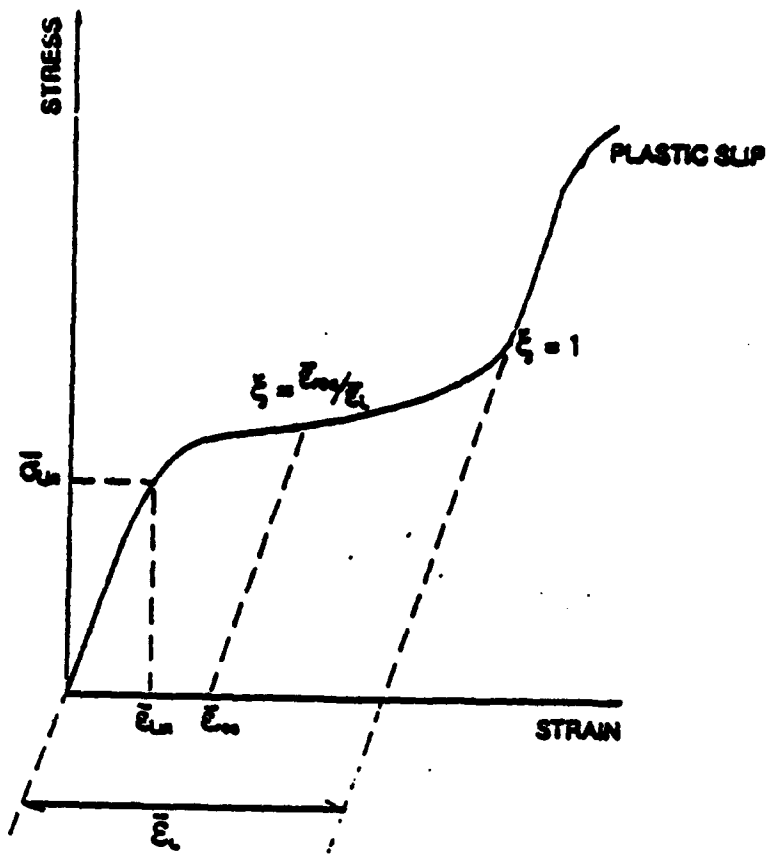

Figure 9. Typical Stress-Strain Relationship of SMA [12].

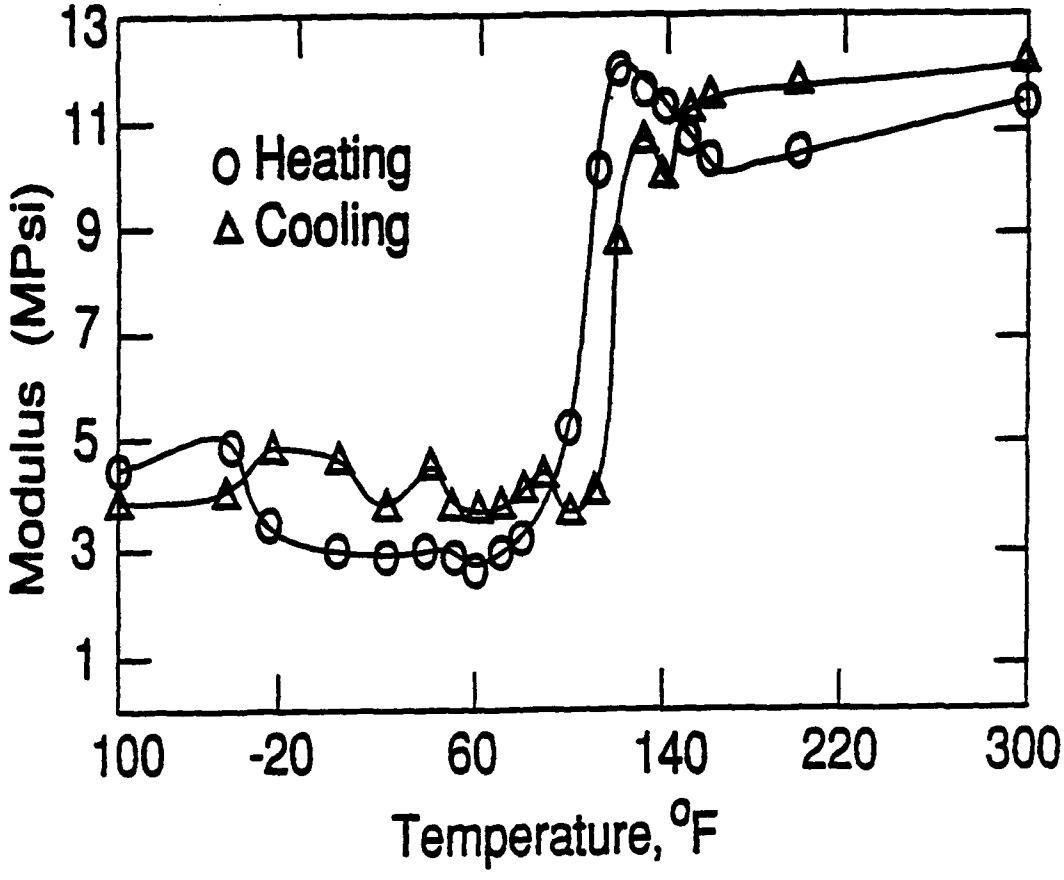

Figure 10. Young's Modulus of a Nitinol Vs. Temperature [12].

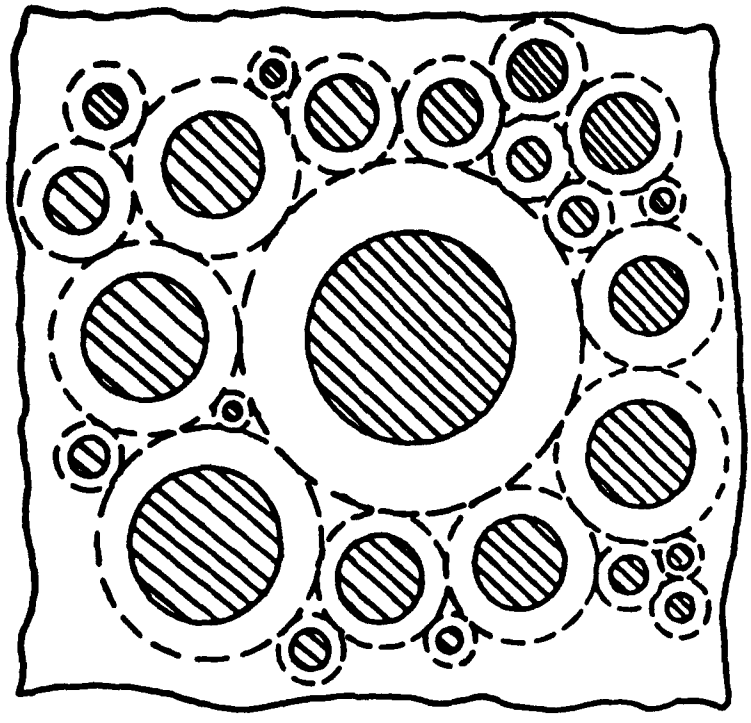

Figure 11. Conceptual Diagram of the Composite Cylinders Assemblage Method [26].

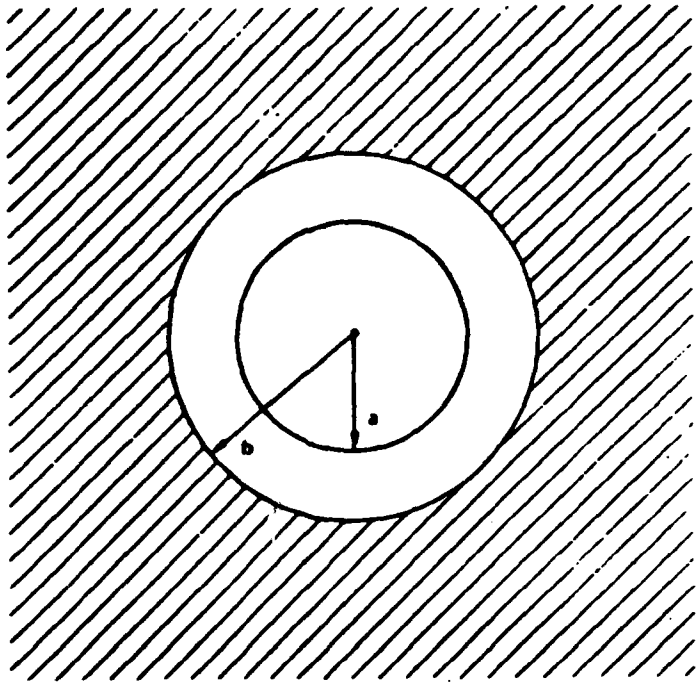

Figure 12. Conceptual Diagram of the Generalized Self-Consistent Scheme [29].

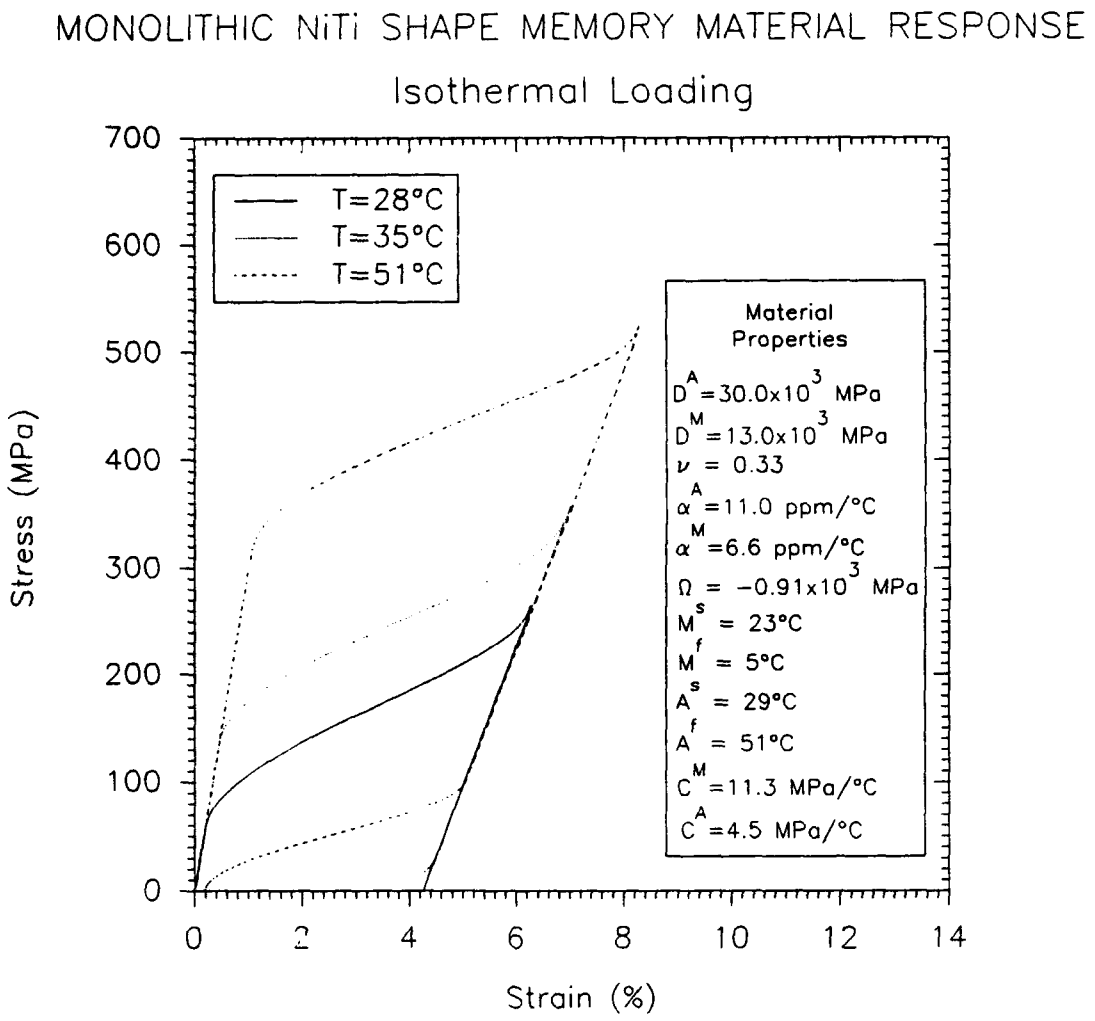

Figure 13. **Axial Stress-Strain Response of Monolithic NiTi SMA Under Isothermal Loading Conditions.**

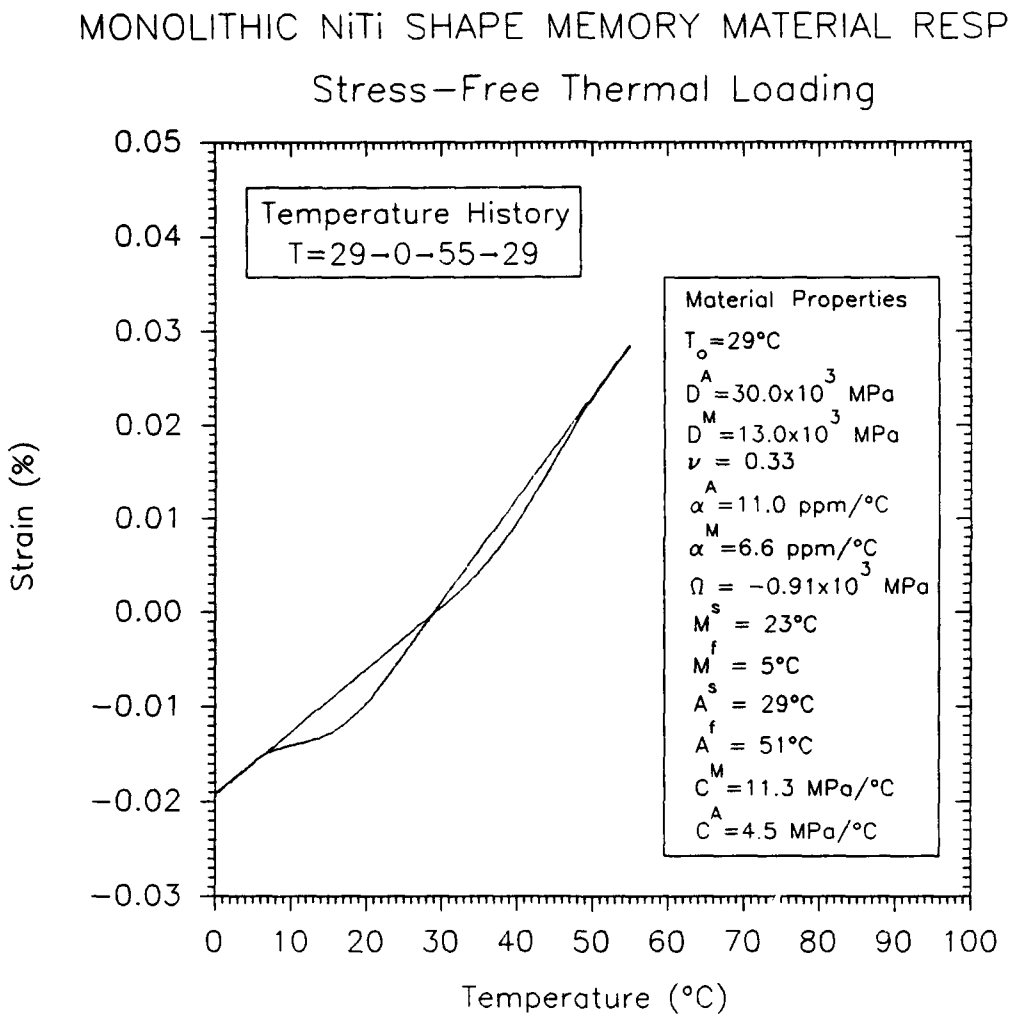

Figure 14. Thermal Strain Versus Temperature Response of Monolithic NiTi SMA Under Stress-Free Conditions.

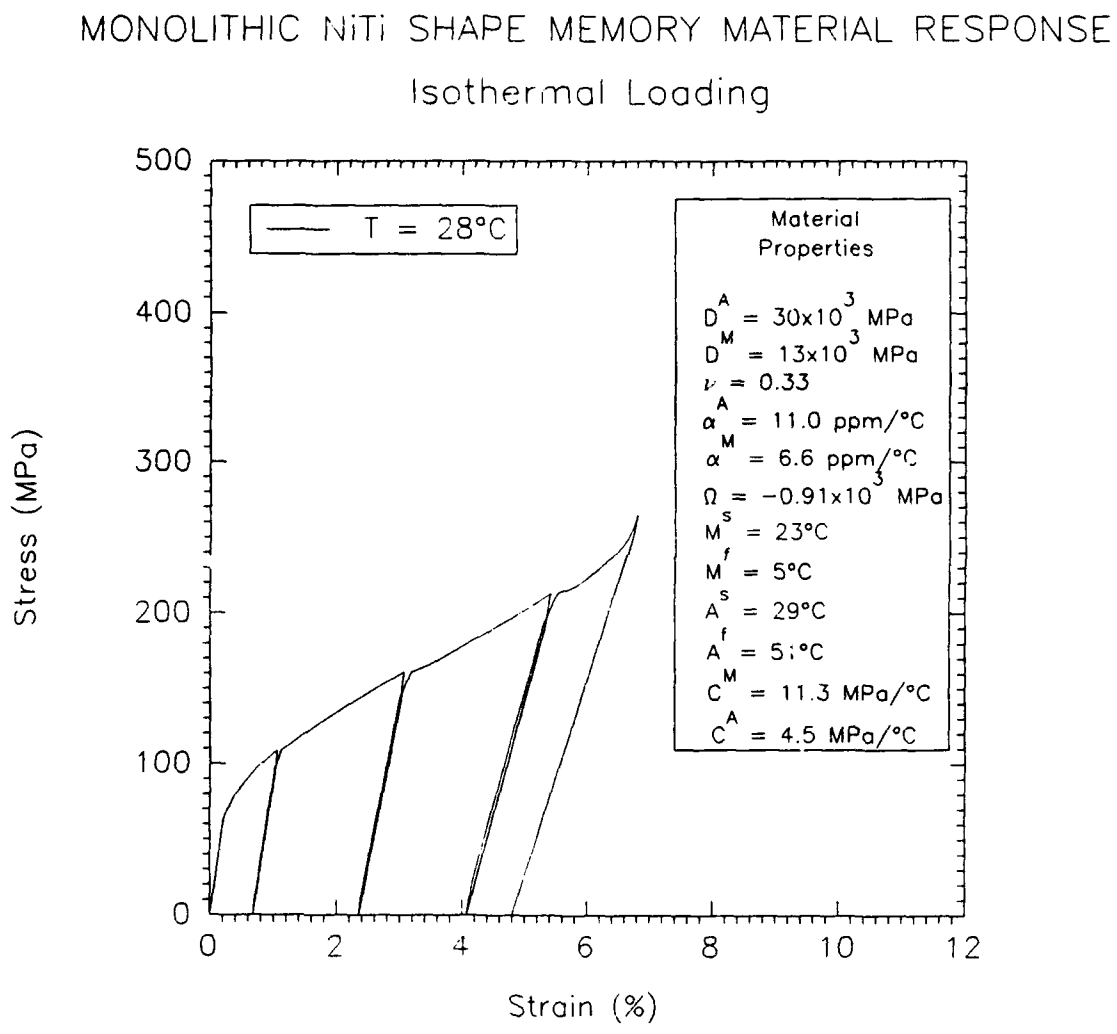

Figure 15. **Phase Change Hardening of Monolithic NiTi SMA Under Isothermal Loading.**

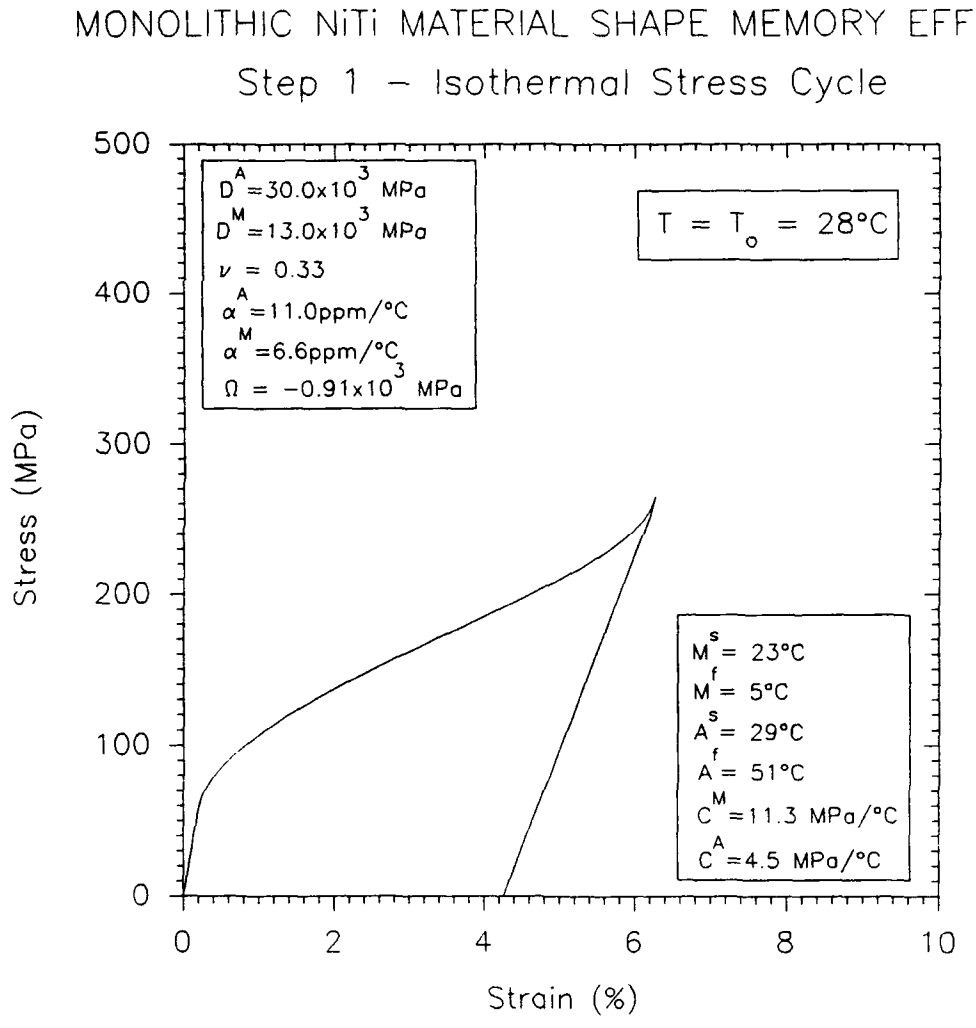

Figure 16. Shape Memory Effect For Monolithic NiTi SMA: Step 1 - Isothermal Stress Cycle.

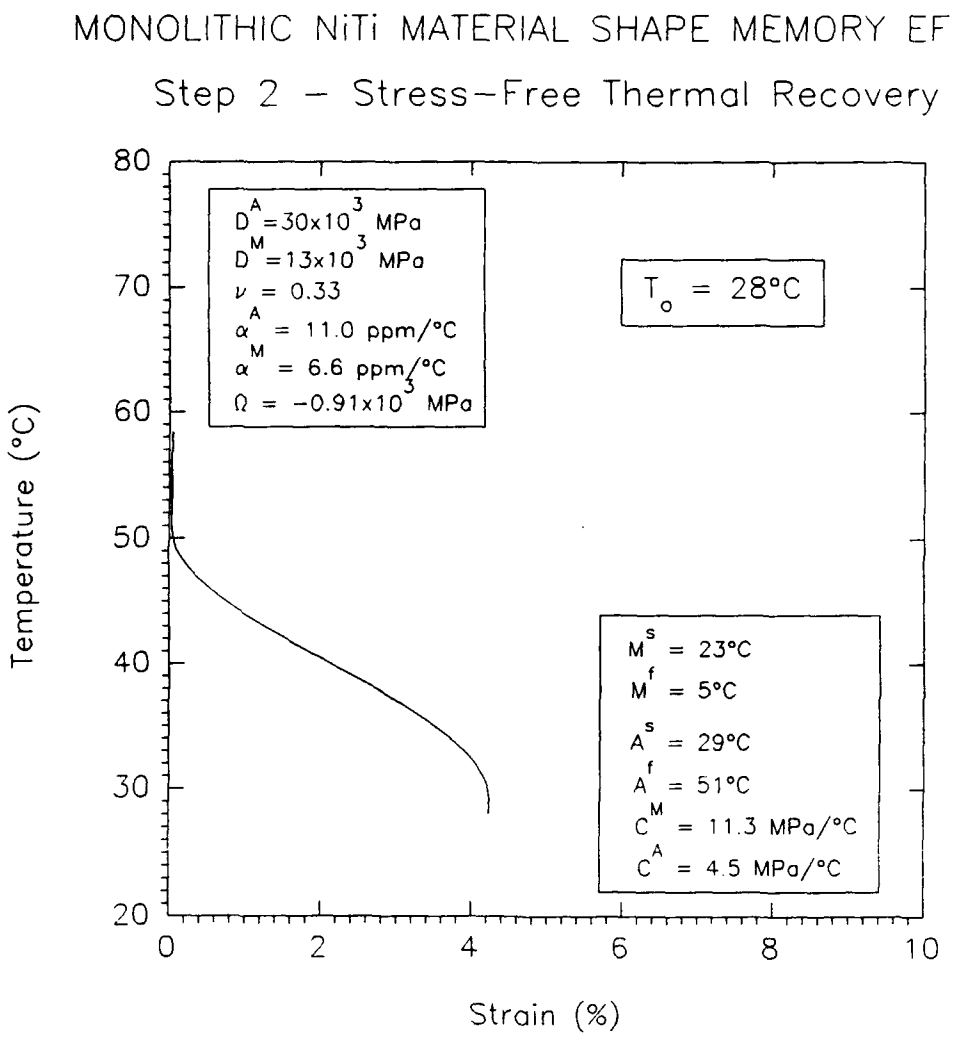

Figure 17. Shape Memory Effect for Monolithic NiTi SMA: Step 2 - Stress-Free Thermal Recovery.

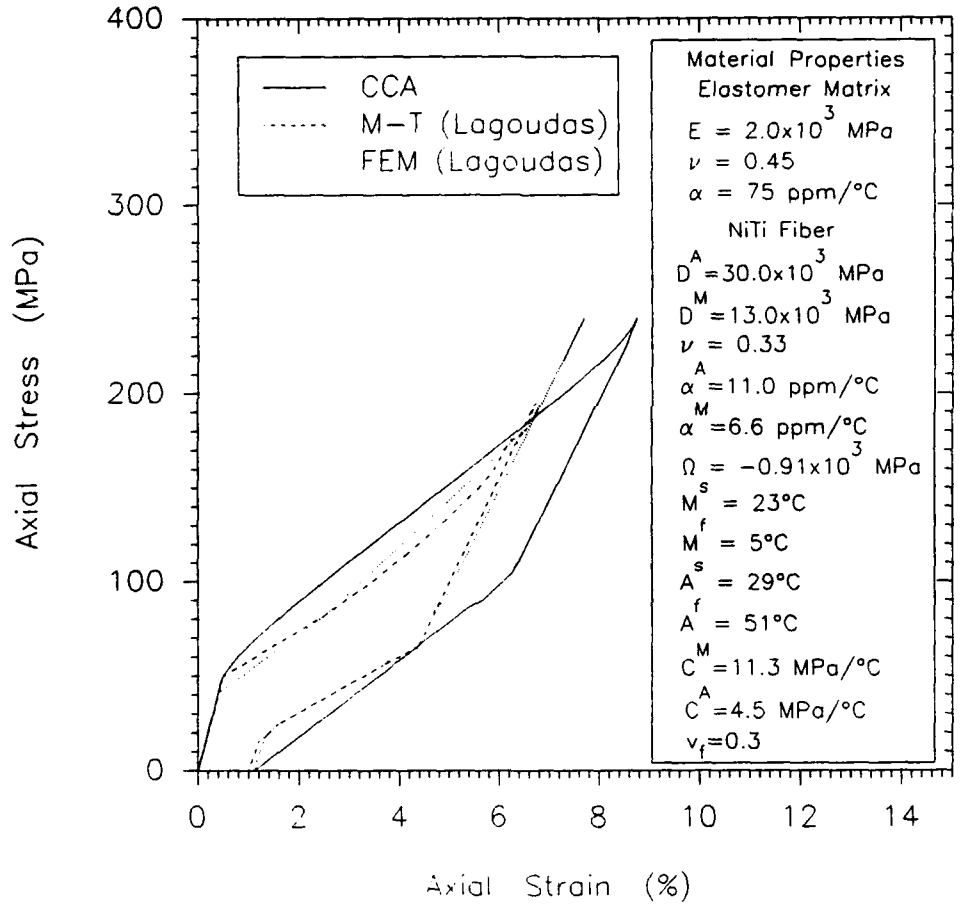

Figure 18. **Axial Stress Versus Axial Strain for Isothermal Loading of Unidirectional Shape Memory Composite.**

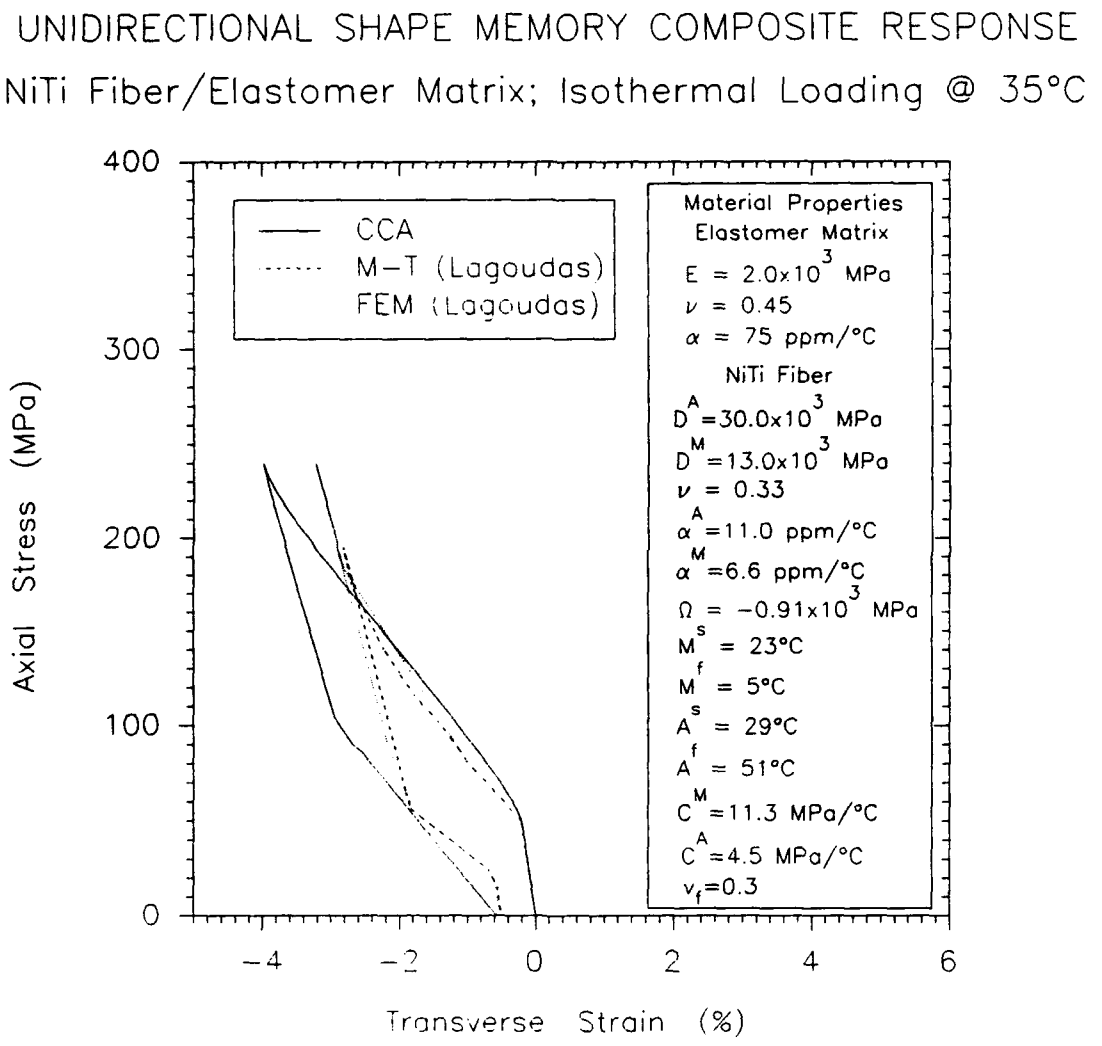

Figure 19. **Axial Stress Versus Transverse Strain for Isothermal Loading of Unidirectional Shape Memory Composite.**

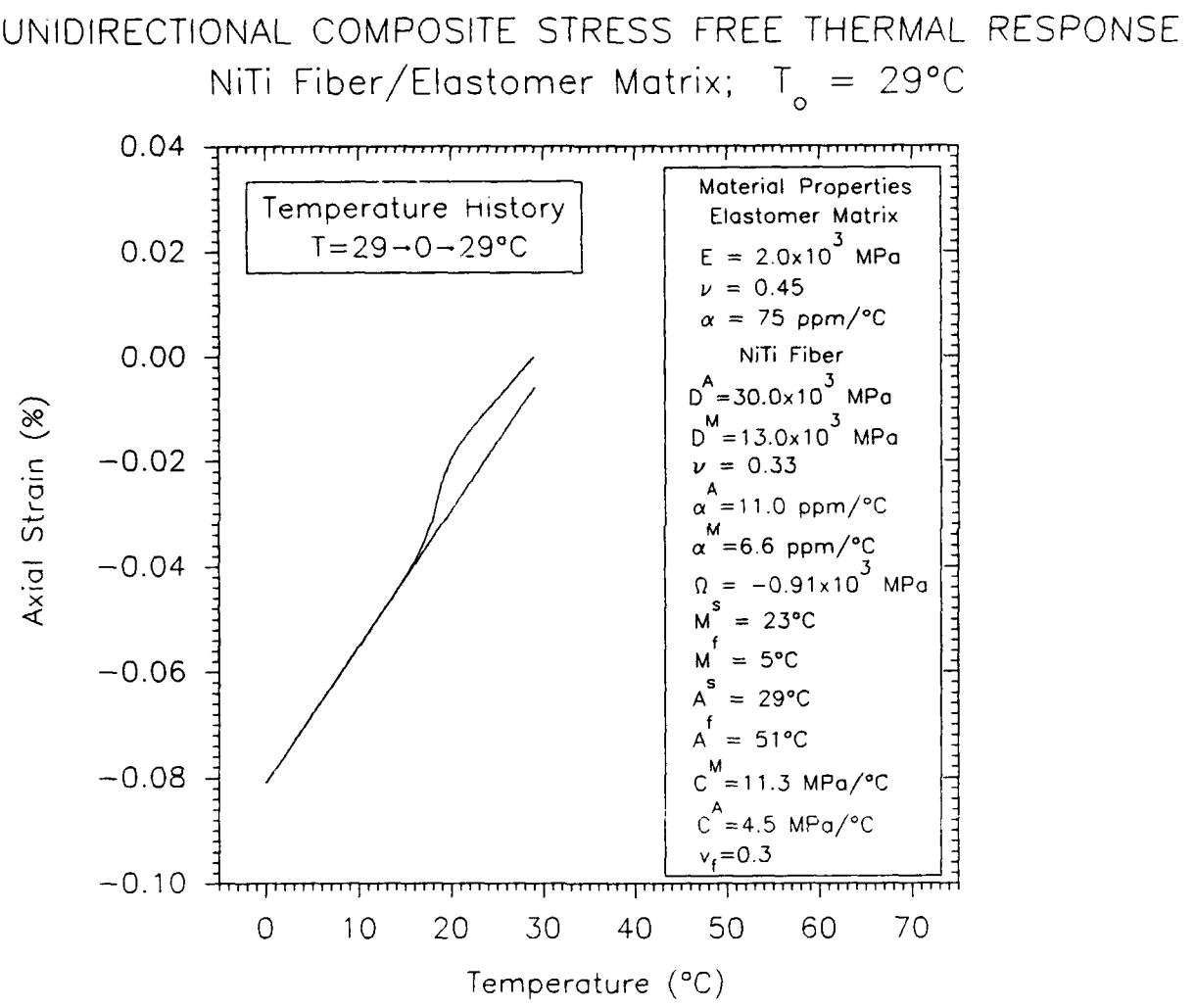

Figure 20. **Composite Stress-Free Thermal Strain Versus Temperature Response for Unidirectional Shape Memory Composite.**

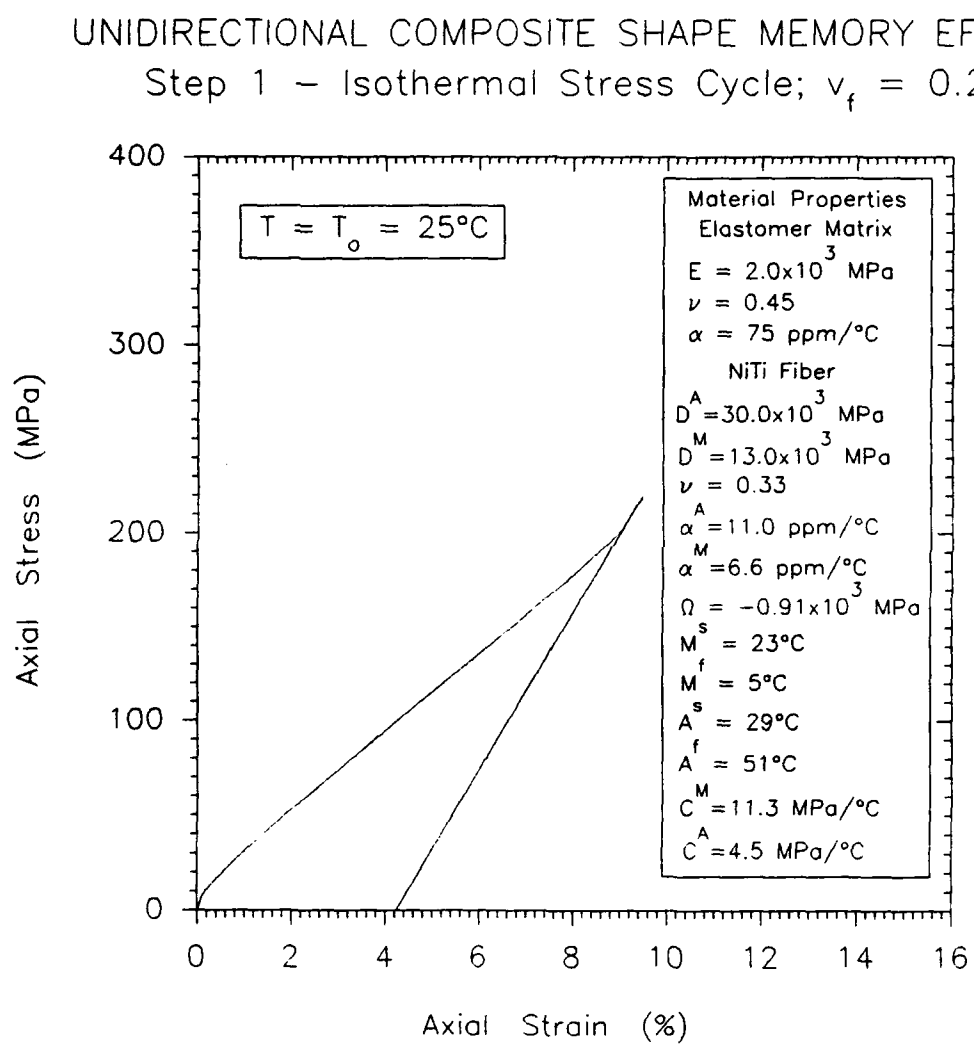

Figure 21. **Shape Memory Effect for Unidirectional NiTi Fiber/Elastomer Matrix Composite at v_f = 0.2; Step 1 - Isothermal Stress Cycle.**

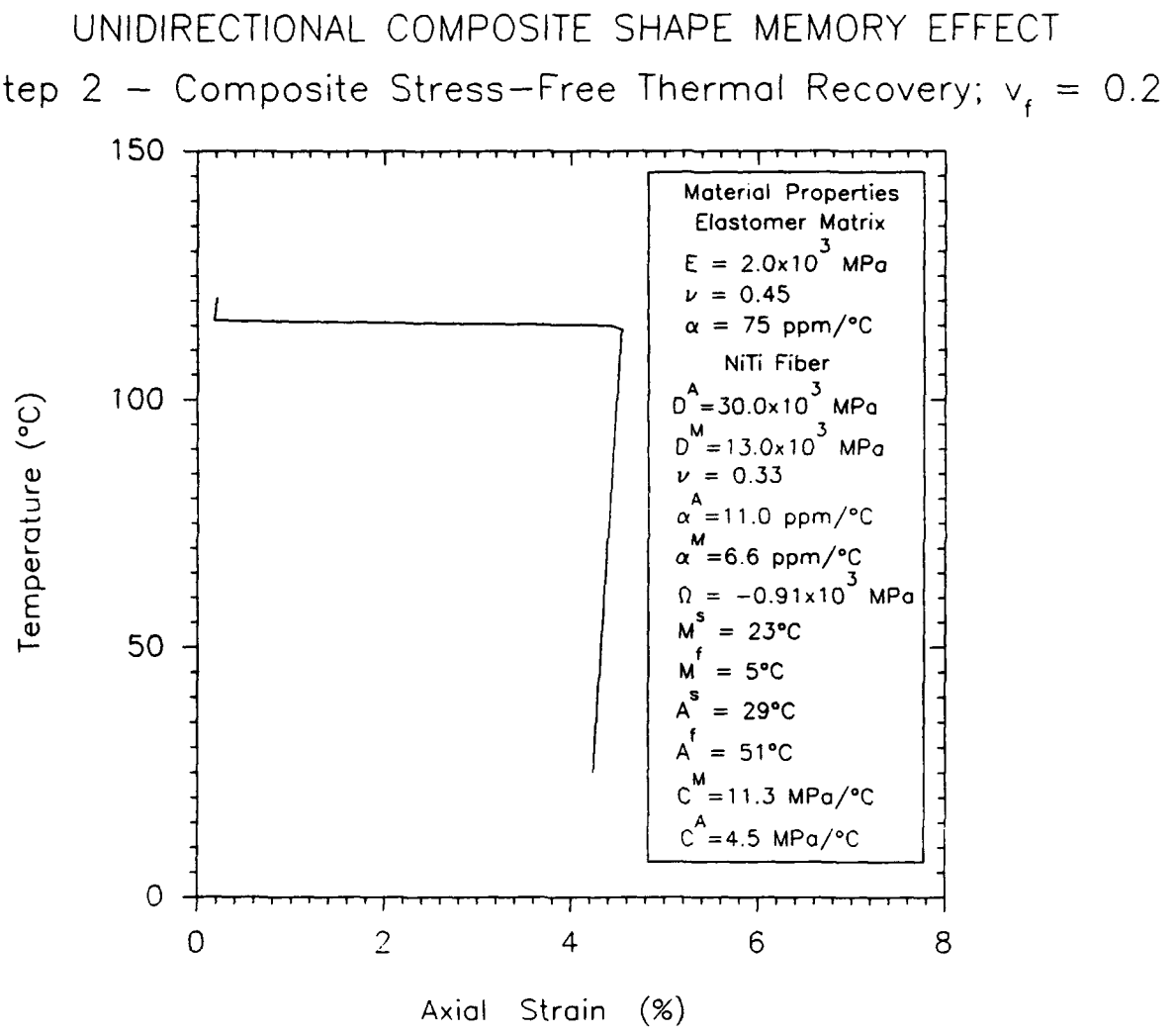

Figure 22. **Shape Memory Effect for Unidirectional NiTi Fiber/Elastomer Matrix Composite at v_f = 0.2; Step 2 - Thermal Recovery.**

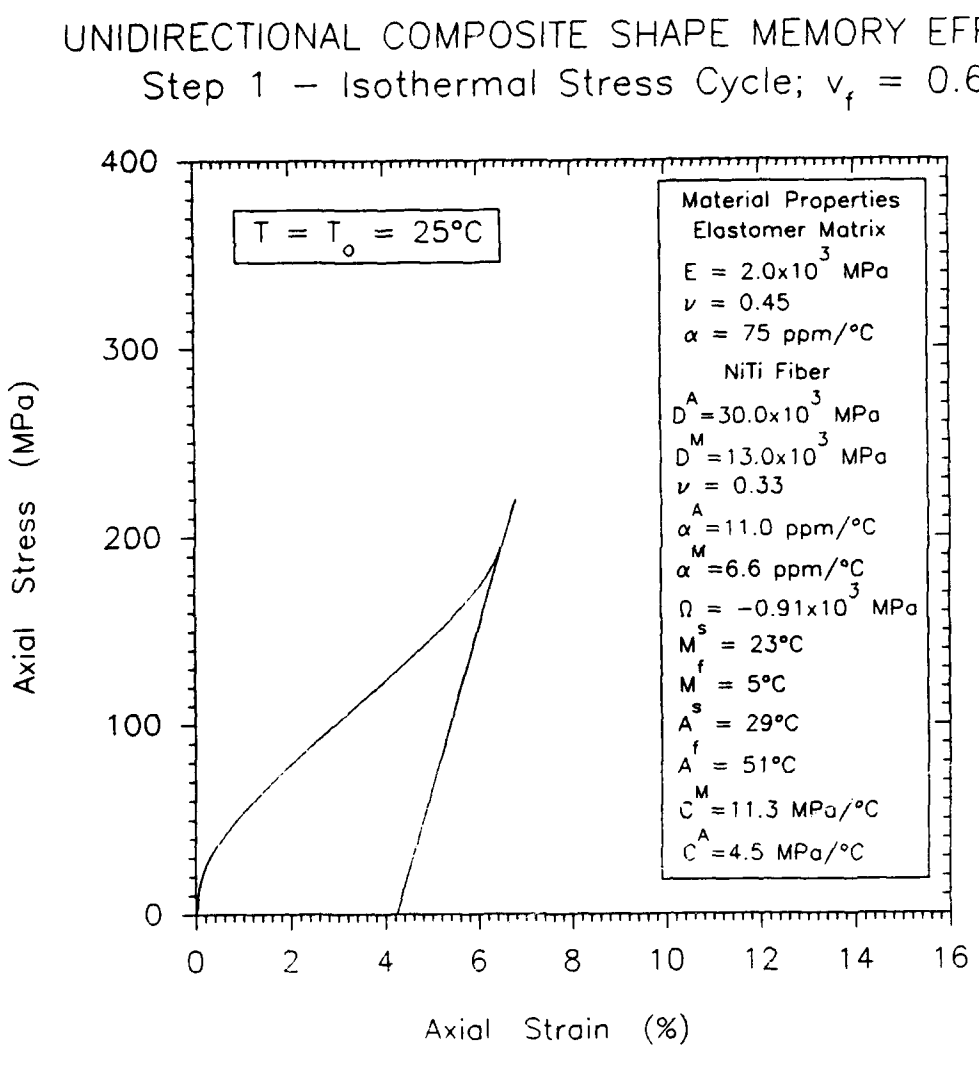

Figure 23. **Shape Memory Effect for Unidirectional NiTi Fiber/Elastomer Matrix Composite at v_f = 0.6; Step 1 - Isothermal Stress Cycle.**

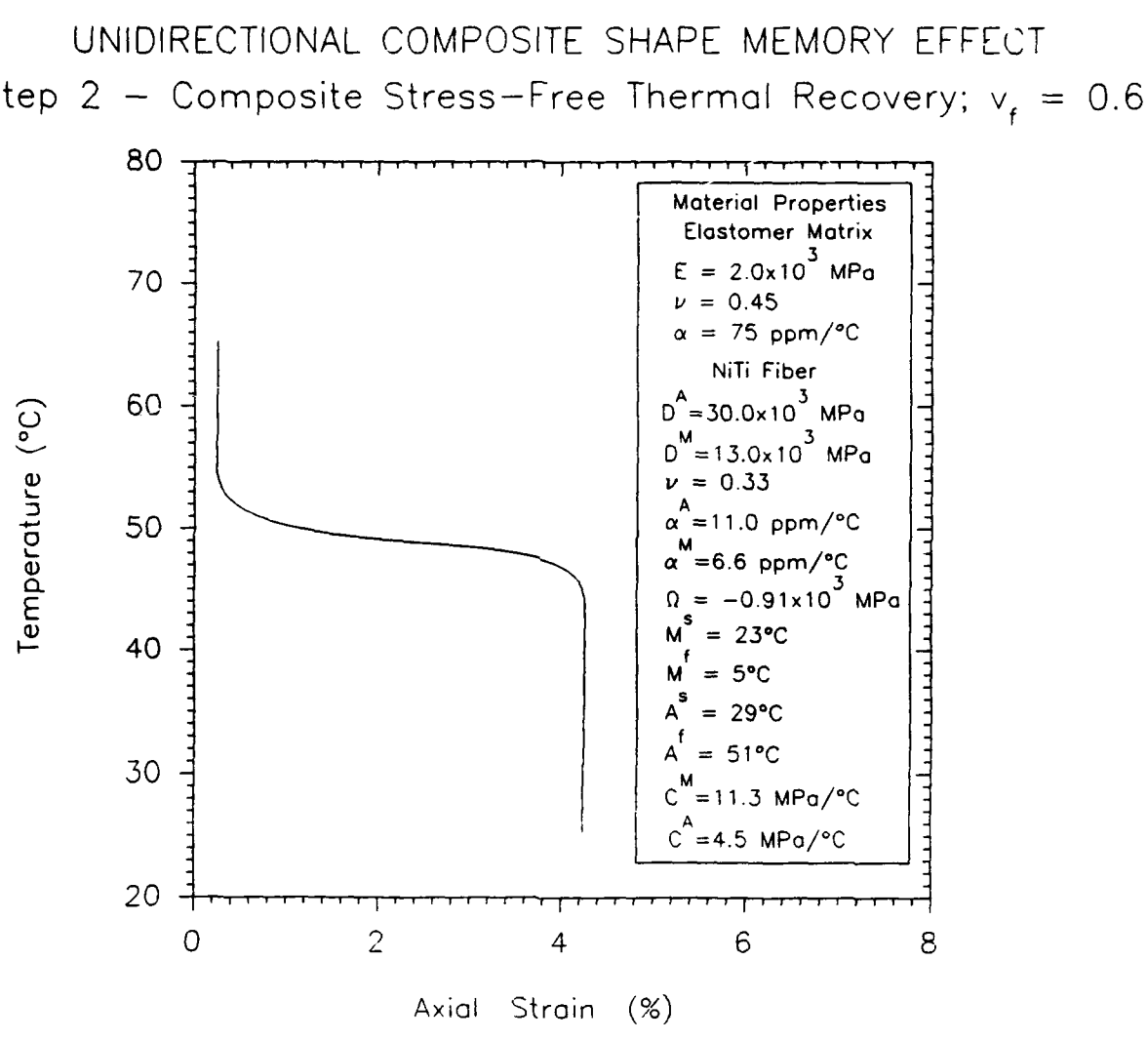

Figure 24. **Shape Memory Effect for Unidirectional NiTi Fiber/Elastomer Matrix Composite at v_f = 0.6; Step 2 - Thermal Recovery.**

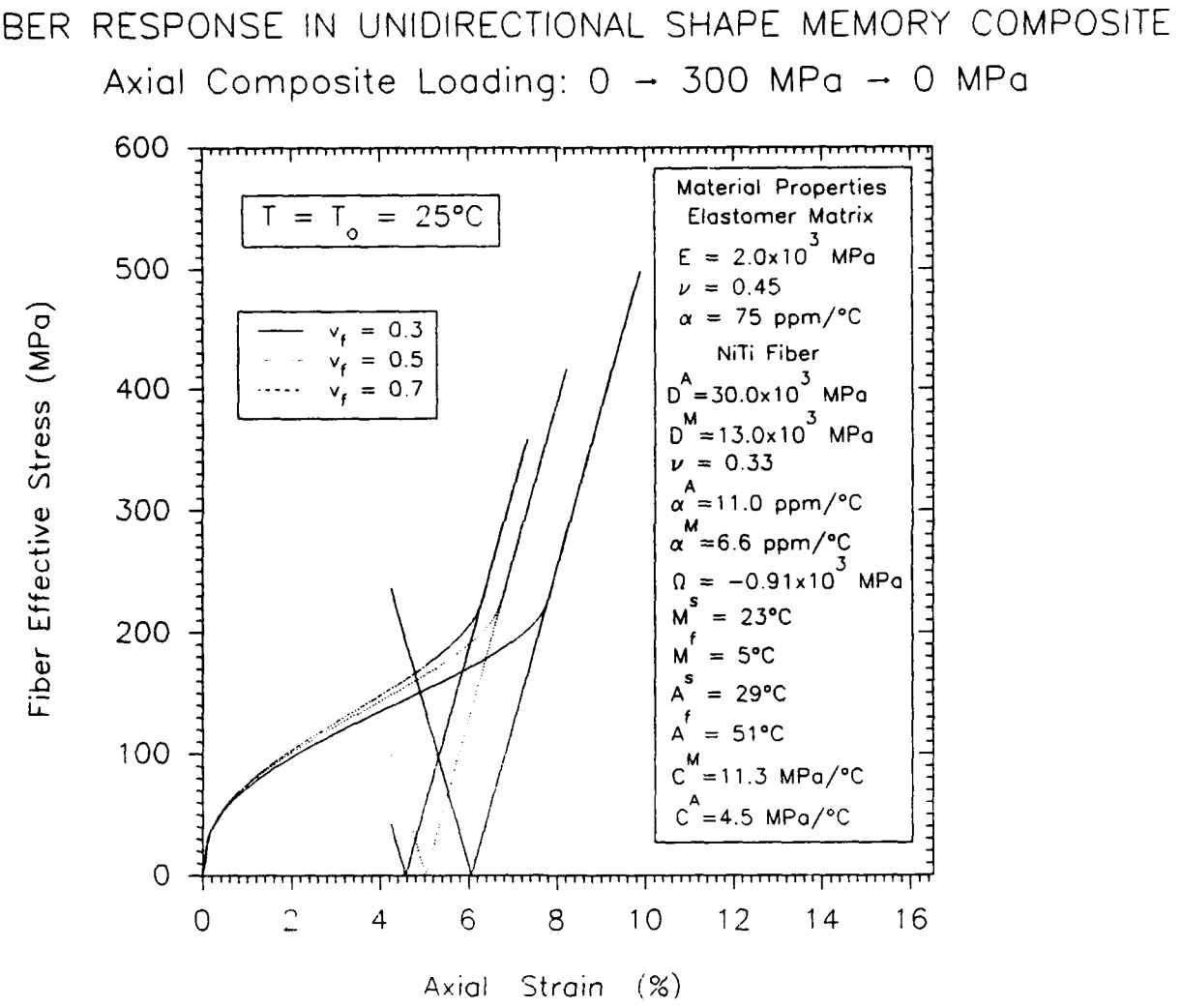

Figure 25. **Fiber Effective Stress Versus Composite Axial Strain for Isothermal Stress Cycle and Different Fiber Volume Fraction Composites.**

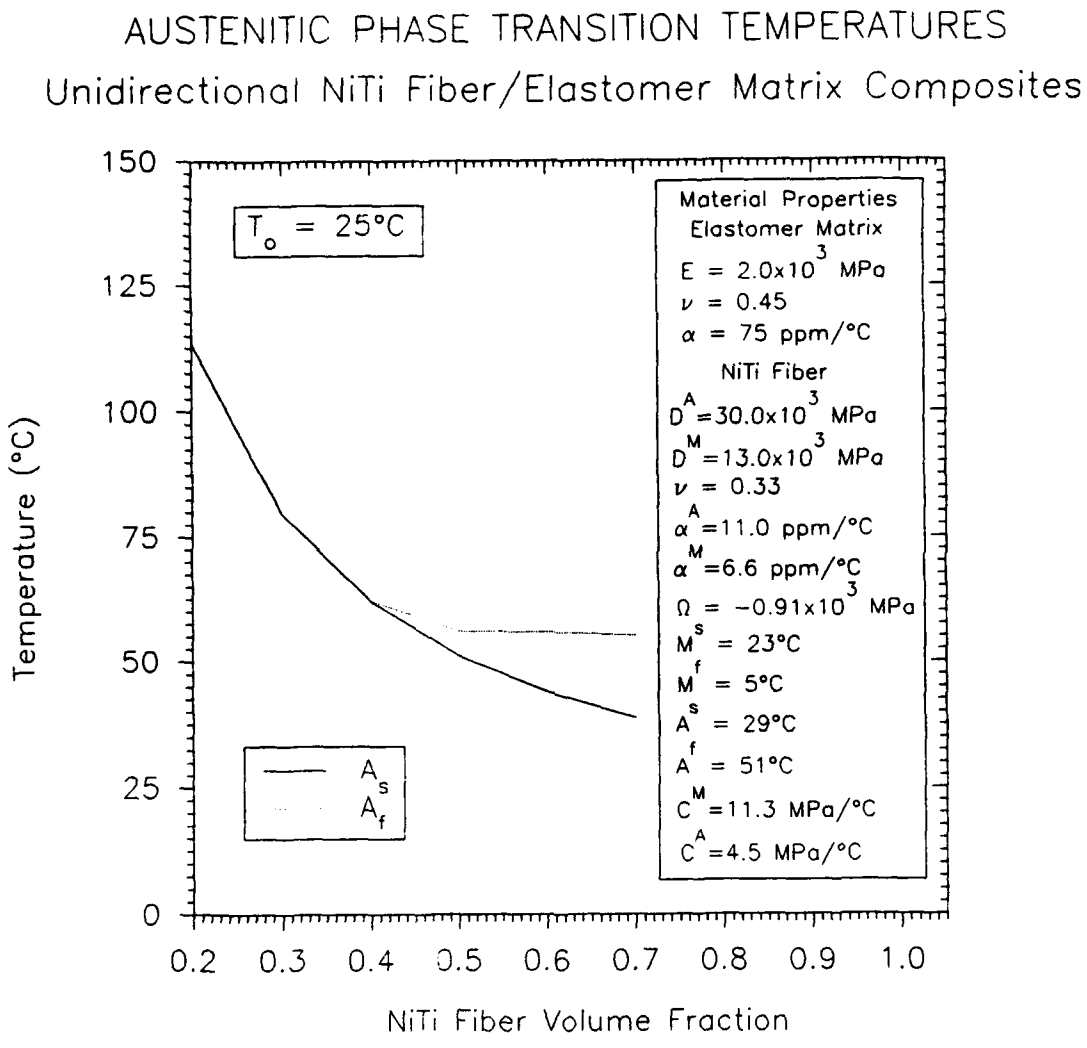

Figure 26. Effective Composite Austenitic Phase Temperatures Obtained From Simulation of the SME Thermal Recovery.

APPENDIX A

Micromechanics of Elastic Fiber/Shape Memory Alloy Matrix Unidirectional Composites

In the case of elastic fiber, shape memory alloy (SMA) matrix composites, the composite shape memory response is obtained from phase transformations occurring within the SMA matrix. Therefore, the matrix stress and strain state must be monitored during thermomechanical loading of the composite. To accomplish this, the rate form of the phase average strain equation

$$\begin{aligned}\dot{\epsilon}^{*}_{ij} &= v_f \dot{\epsilon}^{f}_{ij} + v_m \dot{\epsilon}^{m}_{ij} \\ &= v_f (\dot{\epsilon}^{fe}_{ij} + \alpha^{f}_{ij} \dot{T}) \\ &\quad + v_m (\dot{\epsilon}^{me}_{ij} + \dot{\epsilon}^{mt}_{ij} + \alpha^{m}_{ij} \dot{T} + \dot{\alpha}^{m}_{ij} \Delta T)\end{aligned} \tag{A-1}$$

Using the relations

$$\begin{aligned}\dot{\epsilon}^{fe}_{ij} &= S^{f}_{ijkl} \dot{\sigma}^{f}_{kl} \\ \dot{\epsilon}^{me}_{ij} &= S^{m}_{ijkl} \dot{\sigma}^{m}_{kl} + \dot{S}^{m}_{ijkl} \sigma^{m}_{kl}\end{aligned} \tag{A-2}$$

and also

$$\dot{\epsilon}^{mt}_{ij} = \Lambda^{m}_{ij} \dot{\xi} \tag{A-3}$$

along with the result from the phase average stress rate equation

$$\dot{\sigma}^{f}_{kl} = \frac{1}{v_f} (\dot{\sigma}^{*}_{kl} - v_m \dot{\sigma}^{m}_{kl}) \tag{A-4}$$

equation (A-1) can be rewritten as

$$\begin{aligned}&v_f \left[S^{f}_{ijkl} \cdot \frac{1}{v_f} (\dot{\sigma}^{*}_{kl} - v_m \dot{\sigma}^{m}_{kl}) + \alpha^{f}_{ij} \dot{T} \right] \\ &+ v_m (S^{m}_{ijkl} \dot{\sigma}^{v}_{kl} + \dot{S}^{m}_{ijkl} \sigma^{m}_{kl} + \Lambda^{m}_{ij} \dot{\xi} + \alpha^{m}_{ij} \dot{T} + \dot{\alpha}^{m}_{ij} \Delta T) \\ &= S^{*}_{ijkl} \dot{\sigma}^{*}_{kl} + \dot{S}^{*}_{ijkl} \sigma_{kl} + \Lambda^{*}_{ij} \dot{\xi} + \alpha^{*}_{ij} \dot{T} + \dot{\alpha}^{*}_{ij} \Delta T\end{aligned} \tag{A-5}$$

For the case of an SMA matrix, the martensitic fraction rate is

$$\dot{\xi} = \frac{\partial \xi}{\partial T} \dot{T} + \frac{\partial \xi}{\partial \bar{\sigma}^{m}} \dot{\bar{\sigma}}^{m} \tag{A-6}$$

Substituting (36) and (A-6) into (A-5) and rearranging,

$$
\begin{aligned}
&v_m(S^m_{ijkl}-S^f_{ijkl})\,\dot{\sigma}^m_{kl} + \Big[(S^{A*}_{ijkl}-S^{M*}_{ijkl})\,\sigma^*_{kl} - v_m(S^{Am}_{ijkl}-S^{Mm}_{ijkl})\,\sigma^m_{kl} \\
&\quad - (\alpha^{M*}_{ij}-\alpha^{A*}_{ij}-v_m\alpha^{Mm}_{ij}-v_m\alpha^{Am}_{ij})\,\Delta T - (\Lambda^*_{ij}-v_m\Lambda^m_{ij})\Big]\frac{\partial\xi}{\partial\bar{\sigma}^m}\dot{\bar{\sigma}}^m \qquad \text{(A-7)} \\
&= (S^*_{ijkl}-S^f_{ijkl})\,\dot{\sigma}^*_{kl} + \Big\{(\alpha^*_{ij}-v_m\alpha^m_{ij}-v_f\alpha^f_{ij}) - \Big[(S^{A*}_{ijkl}-S^{M*}_{ijkl})\,\sigma^*_{kl} \\
&\quad - v_m(S^{Am}_{ijkl}-S^{Mm}_{ijkl})\,\sigma^m_{kl} - (\alpha^{M*}_{ij}-\alpha^{A*}_{ij}-v_m\alpha^{Mm}_{ij}-v_m\alpha^{Am}_{ij})\,\Delta T - (\Lambda^*_{ij}-v_m\Lambda^m_{ij})\Big]\frac{\partial\xi}{\partial T}\Big\}\dot{T}
\end{aligned}
$$

The matrix effective stress rate $\dot{\bar{\sigma}}^m$ is expressed in terms of the matrix stress rate tensor $\dot{\sigma}^m_{kl}$ as in (40). Equation (A-7) may then be solved for the $\dot{\sigma}^m_{kl}$ which are then used to compute $\dot{\bar{\sigma}}^m$. The martensitic fraction rate is then computed from (A-6) and equation (42) is used to calculate the composite strain rate tensor $\dot{\epsilon}^*_{ij}$.